Title:

Genome-wide association study and functional validation implicates JADE1 in tauopathy

Authors:

Kurt Farrell[1,2], SoongHo Kim[1,2], Natalia Han[1,2], Megan A. Iida[1,2], Elias Gonzalez[3], Marcos Otero-Garcia[4], Jamie Walker[5], Tim Richardson[5], Alan E. Renton[2,6], Shea J. Andrews[2,6], Brian Fulton-Howard[2,6], Jack Humphrey[2,6], Ricardo A. Vialle[2,6], Kathryn R. Bowles[2,6], Kristen Whitney[1,2], Diana K. Dangoor[1,2], Edoardo Marcora[2,6], Marco M. Hefti[7], Alicia Casella[1,2], Cheick Sissoko[1,2], Manav Kapoor [2,6], Gloriia Novikova[2,6], Evan Udine[2,6], Garrett Wong[2,6],Weijing Tang[30], Tushar Bhangale[8], Julie Hunkapiller[8], Gai Ayalon[9], Rob Graham[10], Jonathan D. Cherry[11], Etty Cortes[1,2], Valeriy Borukov[1,2], Ann C. McKee[11], Thor D. Stein[11], Jean-Paul Vonsattel[12], Andy F. Teich[12], Marla Gearing[13], Jonathan Glass[13], Juan C. Troncoso[14], Matthew P. Frosch[15], Bradley T. Hyman[15], Dennis W. Dickson[16], Melissa E. Murray[16], Johannes Attems[17], Margaret E. Flanagan[18], Qinwen Mao[18], M-Marsel Mesulam[18], Sandra Weintraub[18], Randy Woltjer[19], Thao Pham[19], Julia Kofler[20], Julie A. Schneider[21], Lei Yu[21], Dushyant P. Purohit[1,22], Vahram Haroutunian[22], Patrick R. Hof[2], Sam Gandy[22,38], Mary Sano[22], Thomas G. Beach[23], Wayne Poon[24], Claudia Kawas[39], María Corrada[24], Robert A. Rissman[25], Jeff Metcalf[25], Sara Shuldberg[25], Bahar Salehi[25], Peter T. Nelson[26], John Q. Trojanowski[27], Edward B. Lee[27], David A. Wolk[27], Corey T. McMillan[28], Dirk C. Keene[29], Thomas J. Montine[29,30], Gabor G. Kovacs[31,32,33], Mirjam I. Lutz[33], Peter Fischer[33], Richard J. Perrin[34], Nigel Cairns[37], Erin E. Franklin[34], Herbert T. Cohen[35], Maria Inmaculada Cobos Sillero[30], Bess Frost[3], Towfique Raj[2,6], Alison Goate[2,6], Charles L. White III[36], John F. Crary[1,2]

Grants:
MSSM: R01 AG054008, R01 NS095252, R01 AG060961, and R01 NS086736 Tau Consortium, Genentech/Roche, Alexander Saint-Amand Fellowship (JFC)**,** F32 AG056098 and P30 AG066514 (KF)**,** P50 AG005138 and P30 AG066514 (VH, JFC,MS, SG, AG, PH), 75N95019C00049 (VH) K99 AG070109 (SJA) **BU / MSSM / MAYO:** R01 AG062348 (AM JFC DD) **CUMC:** P50AG008702 (JPV AFT) **BU:** U54 NS115266 (AM) **UPENN:** P30 AG010124, P01 AG017586 and U19 AG062418 (JQT)**,** P30 AG072979 and P01 AG066597 (EBL) **PITT:** R01 AG066152 P30 AG066468 (JK) **Banner :** U24 NS072026 and P30 AG019610 The Arizona Department of Health Services, and the Michael J. Fox Foundation for Parkinson's Research (TB) **Northwestern:** P30 AG013854 (MEF) **Emory:** P30 NS055077 and P50 AG025688 (MG) **OHSU:** P30 AG08017 (RW) **UTSW:** Winspear Family Center for Research on the Neuropathology of Alzheimer Disease (CWIII) **Vienna / Toronto:** Rossy Foundation and by the Safra Foundation (GGK) **MADRC:** BT P50 AG05134 (BH) **RUSH:** ADC grant AG10161 and MAP grant (JS) **UCI:** R01AG021055 and P50AG016573 (CK) **UCSD:** P30 AG062429 01 and P50 AG005131 (RR) **UK:** P30 AG028383 (PN) **U Washington:** AG05136 AG006781 and the Nancy and Buster Alvord Endowment (DK) **Washington U / Knight ADRC:** P30 AG066444, P01 AG003991 and P01 AG026276 (DK) **Other:** J.M.R. Barker Foundation**,** The McCune Foundation

Acknowledgments: The authors would like to acknowledge the neuropathology core of the Massachusetts Alzheimer Disease Research Center, the Biosample Management Repository at Genentech/Roche, the brain repository at UCI, Knight Alzheimer Disease Research Center Neuropathology Core at Washington University School of Medicine, the neurodegenerative disease brain bank at the University of California San Francisco, the Neuropathology Brain Bank & Research Core at Mount Sinai, and the following people: Ryan Cassidy Bohannan, Chad Caraway, Allison Beller, Kim Howard, Suresh Selvaraj, Ward Ortmann, Ping Shang, Jeff Harris, and Chan Foong,

Affiliations:

1 *Department of Pathology, Neuropathology Brain Bank & Research CoRE, Icahn School of Medicine at Mount Sinai, New York NY, USA*

2 *Nash Department of Neuroscience, Friedman Brain Institute, Ronald M. Loeb Center for Alzheimer's Disease, Icahn School of Medicine at Mount Sinai, New York NY USA*

3 *Glenn Biggs Institute for Alzheimer's and Neurodegenerative Diseases, the Sam and Ann Barshop Institute for Longevity and Aging Studies, Department of Cell Systems and Anatomy, University of Texas Health, San Antonio, San Antonio, TX, USA*

4 *Department of Pathology and Laboratory Medicine, Division of Neuropathology, University of California, Los Angeles, CA, USA*

5 *Department of Pathology, UT Health San Antonio Glenn Biggs Institute for Alzheimer's & Neurodegenerative Diseases, San Antonio TX, USA*

6 *Department of Genetics and Genomic Sciences, Icahn School of Medicine at Mount Sinai, New York NY, USA*

7 *Department of Pathology, University of Iowa, Iowa City IA, USA*

8 *Department of Human Genetics, Genentech, San Francisco CA, USA*

9 *Ultragenyx Pharmaceuticals, Novato, CA, USA;*

10 *Maze* Therapeutics, *San Francisco CA, USA*

11 *Department of Pathology (Neuropathology), VA Medical Center & Boston University School of Medicine, Boston MA, USA*

12 *Department of Pathology & Cell Biology and the Taub Institute for Research on Alzheimer's Disease and the Aging Brain, Columbia University Medical Center, New York NY, USA*

13 *Department of Pathology and Laboratory Medicine (Neuropathology)* and Neurology, *Emory University School of Medicine, Atlanta GA USA*

14 *Department of Pathology, Division of Neuropathology, Johns Hopkins University School of Medicine, Baltimore MD, USA*

15 *Department of Neurology and Pathology, Harvard Medical School and Massachusetts General Hospital, Charlestown MA, USA*

16 *Department of Neuroscience, Mayo Clinic, Jacksonville FL, USA*

17 *Institute for Ageing and Health, Newcastle University, Newcastle upon Tyne, UK*

18 *Department of Pathology (Neuropathology), Northwestern Cognitive Neurology and Alzheimer Disease Center, Northwestern University Feinberg School of Medicine, Chicago IL USA*

19 *Department of Pathology, Oregon Health Sciences University, Portland OR, USA*

20 *Department of Pathology (Neuropathology), University of Pittsburgh Medical Center, Pittsburgh PA, USA*

21 *Departments of Pathology (Neuropathology) and Neurological Sciences, Rush University Medical Center, Chicago IL, USA*

22 *Department of Psychiatry, Alzheimer's Disease Research Center, James J. Peters VA Medical Center, Icahn School of Medicine at Mount Sinai, New York, New York, USA*

23 *Neuropathology, Banner Sun Health Research Institute, Sun City AZ, USA*

24 *Department of Neurology, Department of Epidemiology, Institute for Memory Impairments and Neurological Disorders, UC Irvine, Irvine CA, USA*

25 *Department of Neurosciences University of California and the Veterans Affairs San Diego Healthcare System, San Diego, La Jolla, California, USA*

26 *Department of Pathology (Neuropathology) and Sanders-Brown Center on Aging, University of Kentucky, Lexington KY, USA*

27 Center for Neurodegenerative Disease Research, Department of Pathology and Laboratory Medicine, Perelman School of Medicine, University of Pennsylvania, Philadelphia, Pennsylvania, USA

28 Department of Neurology, Perelman School of Medicine, University of Pennsylvania, Philadelphia, Pennsylvania, USA

29 *Department of Laboratory Medicine and Pathology, University of Washington School of Medicine, Seattle, WA, USA (previous address for* Thomas J. Montine)

30 *Department of Pathology, Stanford University, Stanford, USA*

31 *Laboratory Medicine Program & Krembil Brain Institute University Health Network Toronto Ontario Canada*

32 *Tanz Centre for Research in Neurodegenerative Disease and Department of Laboratory Medicine and Pathobiology, University of Toronto, Toronto, Ontario, Canada*

33 *Institute of Neurology, Medical University of Vienna, Vienna, Austria (previous address for Gabor G. Kovacs, Mirjam I. Lutz, Peter Fischer)*

34 *Department of Pathology and Immunology, Washington University School of Medicine, St. Louis MO, USA*

35 *Department of Pathology, Boston University School of Medicine, Boston MA, USA*

36 *Department of Pathology (Neuropathology), University of Texas Southwestern Medical School, Dallas TX, USA*

37 *College of Medicine and Health, University of Exeter, Exeter, UK*

38 *Department of neurology, center for cognitive health, Icahn School of Medicine at Mount Sinai, New York NY, USA*

39 *Department of Neurology, Department of Neurobiology & Behavior, Institute for Memory Impairments and Neurological Disorders, UC Irvine, Irvine CA, USA*

Abstract

Primary age-related tauopathy (PART) is a neurodegenerative tauopathy with features distinct from but also overlapping with Alzheimer disease (AD). While both exhibit Alzheimer-type temporal lobe neurofibrillary degeneration alongside amnestic cognitive impairment, PART develops independently of amyloid-β (Aβ) deposition in plaques. The pathogenesis of PART is unknown, but evidence suggests it is associated with genes that promote tau pathology as well as others that protect from Aβ toxicity. Here, we performed a genetic association study in an autopsy cohort of individuals with PART (*n*=647) using Braak neurofibrillary tangle stage as a quantitative trait adjusting for sex, age, genotyping platform, and principal components. We found significant associations with some candidate loci associated with AD and progressive supranuclear palsy, a primary tauopathy (*SLC24A4*, *MS4A6A*, *HS3ST1*, *MAPT* and *EIF2AK3*). Genome-wide association analysis revealed a novel significant association with a single nucleotide polymorphism on chromosome 4 (rs56405341) in a locus containing three genes, including *JADE1* which was significantly upregulated in tangle-bearing neurons by single-soma RNA-seq. Immunohistochemical studies using antisera targeting JADE1 protein revealed localization within tau aggregates in autopsy brain from tauopathies containing isoforms with four microtubule-binding domain repeats (4R) and mixed 3R/4R, but not with 3R exclusively. Co-immunoprecipitation revealed a direct and specific binding of JADE1 protein to tau containing four (4R) and no N-terminal inserts (0N4R) in post-mortem human PART brain tissue. Finally, knockdown of the *Drosophila* JADE1 homolog rhinoceros (rno) enhanced tau-induced toxicity and apoptosis *in vivo* in a humanized 0N4R mutant tau knock-in model as quantified by rough eye phenotype and terminal deoxynucleotidyl transferase dUTP nick end-labeling (TUNEL) in the fly brain. Together, these findings indicate that PART has a genetic architecture that partially overlaps with AD and other tauopathies and suggests a novel role for JADE1 as a mediator of neurofibrillary degeneration.

Introduction

Primary age-related tauopathy (PART) is nearly ubiquitously observed with varying degrees of severity in the brains of aged individuals characterized by the presence of neurofibrillary tangles (NFT) composed of abnormal aggregates of tau protein. These NFTs are regionally, morphologically, biochemically and ultrastructurally identical to those in early to moderate stage Alzheimer disease (AD), yet develops in the absence of Aβ plaques [1]. A neuropathological diagnosis of PART is separate from a clinical diagnosis of cognitive impairment; hence individuals with PART can be normal, mildly cognitively impaired (MCI) or have dementia [2,3]. Most individuals with PART remain cognitively normal, however some develop amnestic cognitive changes [4-7]. The similarities between PART and AD allows for a unique opportunity to focus specifically on mechanisms of tau-mediated AD-type neurodegeneration. The neuropathological diagnosis of PART is complicated by accompanying age-related comorbid dementing pathologies, therefore discovering unique molecular drivers is challenging antemortem [8-13]. Given the similarities between PART and AD NFTs, PART as a diagnostic construct would have greater value if it were shown to arise independently [14,15]. Alternatively, PART might be a component of the AD spectrum, and Aβ pathology might have eventually developed in such individuals had they lived longer [15,16]. Thus, the question remains as to what extent a neuropathological diagnosis of PART diverges from or has similar risk factors to AD and other dementias [17,18].

Much of the mechanistic knowledge surrounding tauopathy stems from genetic studies [19]. Autosomal dominant mutations in the microtubule-associated protein tau gene (*MAPT*) in coding regions can interfere with microtubule binding or promote transition to toxic forms. Also, mutations in splice sites disrupt alternative pre-mRNA splicing of the tau mRNA transcript, modifying the ratio of three repeat (3R) and four repeat (4R) tau isoforms leading to downstream pathological sequelae [20]. Additionally, alternative splicing of the N-terminal exons may also play a role in modulating toxic tau [21,22]. However, *MAPT* mutations are rare, whereas PART occurs sporadically and nearly ubiquitously with advanced age. Thus, PART provides a unique opportunity to understand common genetic drivers of tauopathy and their association with abnormalities in tau proteostasis and isoform expression. Prior research focusing on common genetic variation has identified two distinct haplotypes in the *MAPT* 17q21.31 locus defined by a large ~900kb inversion region that gives rise to two major haplotypes, H1 and H2. The more common H1 haplotype has

been associated with increased risk for PART and several other sporadic tauopathies including *APOE* ε4-negative AD, progressive supranuclear palsy, corticobasal degeneration, and even Parkinson disease which is not classically considered a tauopathy [23-28]. Research focusing on the genetics of PART have consistently failed to show an association with the *APOE* ε4 allele, the strongest risk locus in AD [28-31]. Outside of PART, one of the largest AD GWAS has identified 29 risk loci implicating 215 potential causative genes [32]. However, it has been suggested that the overwhelmingly strong signal on the *APOE* locus could mask associations independently related to tauopathy [23]. Another study examining candidate genes in aging cohorts confirmed the lack of the association between *APOE* ε4 and PART, as well as a decreased frequency of AD risk alleles in the *BIN1*, *PTK2B*, and *CR1* loci [33]. Taken together, these data suggest an unexplored genetic risk driving tauopathy that might be revealed by conducting genome-wide association studies in PART.

While PART represents a compelling opportunity to focus on amyloid-independent mechanisms of neurofibrillary degeneration, assembling an autopsy cohort large enough to assesses its genetics on a genome-wide scale has not yet been attempted. In collaboration with twenty-one domestic and international brain biorepositories, we performed the first genome-wide association study in PART and compared our findings to known tauopathy risk loci. We then localized expression of candidate genes in our strongest risk locus (chromosome 4q28.2) using single cell RNA-sequencing and immunohistochemistry. Finally, we validated our findings biochemically in human postmortem brain and functionally using an *in vivo* Drosophila model. The work presented here not only furthers the investigation of the genetics of PART, but also suggests a novel role for *JADE1* in tauopathy.

Materials and methods

Cohort

Fresh-frozen brain tissue was obtained from the contributing centers (Supplementary Table 1). All tissue was used in accordance with the relevant guidelines and regulations of the respective institutions. The neuropathological assessments were performed at the respective centers using standardized criteria outlined by the National Institutes on Aging-Alzheimer's Association (NIA-AA) and National Alzheimer Coordinating Center (NACC) which has a high degree of interrater reliability among centers [34,35]. Inclusion criteria were individuals with normal cognition, mild cognitive impairment (any type) and dementia. Cognitive status was determined either premortem or postmortem by a clinical chart review, mini-mental score, or clinical dementia rating [36,37]. Both sexes were included and ages ranged from 51 to 108 years at death. Neuropathological inclusion criteria were Braak tangle stage of 0-IV and neuritic amyloid plaque severity CERAD score of 0 [38,39]. In addition, tissue sections were obtained and reevaluated by the study investigators to confirm the lack of amyloid and degree of PART tau pathology[40]. Clinical exclusion criteria were motor neuron disease, parkinsonism, and frontotemporal dementia. Neuropathological exclusion criteria were other degenerative diseases associated with NFTs (i.e., AD, progressive supranuclear palsy [PSP], corticobasal degeneration [CBD], chronic traumatic encephalopathy [CTE], frontotemporal lobar degeneration-tau [FTLD-tau], Pick disease, Guam amyotrophic lateral sclerosis/parkinsonism-dementia, subacute sclerosing panencephalitis, globular glial tauopathy). Individuals with aging-related tau astrogliopathy (ARTAG) were not excluded [41].

Genotyping

High-throughput isolation of DNA was performed using the MagMAX DNA Multi-Sample Ultra 2.0 Kit on a KingFisher Flex robotic DNA isolation system (Thermofisher, Waltham, MA). Fresh frozen cortical brain tissue (20-40 mg) was placed into a deep-well plate and treated with 480 µl of Proteinase K mix (Proteinase K, phosphate buffered saline [pH 7.4], Binding Enhancer) and incubated overnight at 65°C at 800 rpm on a shaking plate. Genomic DNA was isolated and purified using magnetic particles. DNA quality control was performed using a nanodrop spectrophotometer (concentration > 50ng/µl, 260/280 ratio 1.7-2.2). Genotyping was performed using single nucleotide polymorphism (SNP) microarrays (Infinium Global

Screening Array v2.4. or Infinium OmniExpress-24; Illumina, San Diego, CA). Raw genotype files were converted to PLINK-compatible files using GenomeStudio software (Illumina, San Diego, CA).

Genetic analysis

PLINK v1.9 was used to perform quality control [42]. SNP exclusion criteria included minor allele frequency <1%, genotyping call-rate filter less then 95%, and Hardy-Weinberg threshold of 1×10^{-6} [43]. Individuals with discordant sex, non-European ancestry, genotyping failure of >5%, or relatedness of >0.1 were excluded. A principal component analysis (PCA) was performed to identify population substructure using EIGENSTRAT and the 1000 genomes reference panel [44,45]. Samples were excluded if they were five standard deviations away from the European population cluster (Supplementary Fig. 4). PCA was performed again on the genomic data with non-Europeans excluded to generate new PCs, of which the first four were used as covariates in the regression model. All data was imputed on the University of Michigan server using minimac3 and HRC reference panel [46,47]. Imputed variants with MAF <0.01 and a dosage R^2 <0.7 were excluded. Downstream analyses were based on the most likely genotype. A quantitative trait association test was run on 647 PART cases vs. Gaussian-normalized Braak stage using conditional linear regression and age, sex, principal component 1-4 and SNP chip array as covariates. The analysis was run separately on each genotyping array and a meta-analysis was performed using METAL [48]. Regional genome-wide association plots were created with LocusZoom, other plots were created using R [49].

Single-cell mRNA profiling in tangle-containing neurons

Identification of differentially expressed genes in single neuronal somata with and without NFTs was performed by analyzing a transcriptomic dataset of isolated neurons from post-mortem human brain from individuals with and without AD reported by Otero-Garcia *et. al*. 2021 [50]. This dataset consists of single neuronal soma transcriptomes from Brodmann area 9 subjected to fluorescence-activated cell sorting (FACS) using p-tau (AT8) and MAP2 antisera to differentiate single NFT-positive and NFT-negative cells.

Immunohistochemistry

Formalin-fixed paraffin-embedded tissue sections (5 µm) on charged slides were baked at 70ºC and immunohistochemistry (IHC) was performed on a Ventana Benchmark XT automatic stainer (Rouche, Tucson, AZ). Antigen retrieval was done using citric acid buffer (CC1) for 1 hr followed by primary antibody incubation for approximately 40 min. A secondary antibody, 3,3'-diaminobenzidine (DAB) was then applied. For slides that were doubled-labeled DAB and alkaline phosphatase were used for visualization. Slides were stained with antibodies to JADE1 (1:100, Proteintech, Rosemont, IL) and hyperphosphorylated tau (p-tau, AT8, 1:1000, Invitrogen, Waltham, MA). To ensure specificity of the JADE1 antisera, a peptide competition was performed using a blocking peptide. The antisera and paired peptide were pre-incubated for 24 hr. Whole slide images (WSI) were visualized and scanned using an Aperio CS2 digital slide scanner (Leica Biosystems, Wetzlar Germany). In addition to PART cases, neuropathologically confirmed cases of AD, PSP, CTE, CBD, argyrophilic grain disease (AGD) and Pick disease (PiD) (*n*=3 for each, Supplemental table 6) were examined for convergent or divergent staining patterns.

Biochemical analysis

Western blots were performed using homogenized fresh-frozen brain tissue. Samples were placed in a micro-tube homogenizer (SP Bel-Art, Wayne, NJ) in 10 volumes (wt/vol) of ice-cold Pierce RIPA buffer (Thermo Fisher Scientific, Waltham, MA) containing Halt protease and phosphatase inhibitor cocktail (Thermo Fisher Scientific), and incubated on ice for 30 min. For each sample, 20 µg of proteins were boiled in 1x Laemmli sample buffer (Bio-Rad, Hercules, CA) for 5 min, run on 10% Criterion TGX Precast Gels (Bio-Rad, Hercules, CA), blotted to nitrocellulose membranes, and stained with JADE1 antisera (1:2000). Horseradish peroxidase-labeled secondary anti-rabbit antisera (1:20,000; Vector Labs, Burlingame, CA) was detected by SuperSignal West Pico PLUS Chemiluminescent Substrate or Pierce ECL Western Blotting Substrate (Thermo Fisher Scientific). To quantify and standardize protein levels, GAPDH was detected with GAPDH antisera (6C5, 1:20,000; Abcam, Cambridge, MA) and total protein was detected with Amido Black (Sigma-Aldrich, St. Louis, MO) as previously described [51]. Chemiluminescence was measured in a ChemiDoc Imaging System (Bio-Rad), and relative optical densities were determined by using AlphaEaseFC software, version 4.0.1 (Alpha Innotech, San Jose, CA), normalized to GAPDH and total protein loaded.

Co-immunoprecipitation (IP) assays were performed using fresh-frozen brain tissue was homogenized in a glass-Teflon homogenizer at 500 rpm in 10 volumes (wt/vol) of ice-cold lysis buffer containing 50 mM Tris, pH 7.8, 0.5 % NP40, 150 mM NaCl, 1 mM EDTA, and Halt protease and phosphatase inhibitor cocktail (Thermo Fisher Scientific). Samples were incubated on ice for 30 min, centrifuged at 1000 x g for 10 min and the supernatant was collected as an input and used for immunoprecipitation. In a microcentrifuge tube, 70 ul of supernatant, Lysis buffer (930 µl) and 2 µg of either JADE1 antisera or anti-0N tau antisera (EPR21726, Abcam, Cambridge, MA) were combined and incubated overnight at 4 °C. Two controls were also set up, one without the antisera and the other with 2 µg of IgG isotype control antisera, either normal rabbit IgG (PeproTech, Rocky Hill, NJ) or Mouse IgG1 kappa, (clone: P3.6.2.8.1, Thermo Fisher Scientific). Twenty µl of Pierce Protein A/G Agarose beads (Thermo Fisher Scientific) was added to each reaction, and the mixture was incubated for 1 hr at 4 °C. Agarose beads were pelleted at 1000 x g for 5 min at 4 °C, supernatant was removed, 1 ml of ice-cold lysis buffer was added, and pellet was washed by inverting tube several times. Beads were washed 4 times, each time repeating the centrifugation step above. After the final wash, pelleted beads were resuspended in 40 µl of 1x Laemmli sample buffer (Bio-Rad, Hercules, CA) and boiled for 5 min. The samples were then centrifuged to pellet the agarose beads followed by SDS-PAGE analysis of the supernatant. Fifteen µl of samples for JADE1 detection and 5 µl for tau with tau isoform ladders (rPeptide, Watkinsville, GA) were run on 10% PROTEAN TGX Precast Gels (Bio-Rad, Hercules, CA), blotted to nitrocellulose membranes, and stained with JADE1 antisera (1:2000), total tau antisera (HT7, 1:3000; Thermo Fisher Scientific), three microtubule repeat domain tau antisera (3R, 8E6/C11, 1:2000; MilliporeSigma, St. Louis, MO), four microtubule repeat domain tau antisera (4R, 1:2000; Cosmo Bio, Carlsbad, CA), pThr231 tau antisera (RZ3, 1:200; a gift from Dr. Peter Davies), pThr181 tau antisera (PHF1, 1:500; a gift from Dr. Peter Davies), pSer202 tau antisera (CP13, 1:500; a gift from Dr. Peter Davies), pSer202/pThr305 tau antisera (AT8, 1:1000; Thermo Fisher Scientific), pSer214 tau antisera (S214; 44-742G, 1:1000; Thermo Fisher Scientific, Waltham, MA), or pSer409 tau antisera (PG5, 1:200; a gift from Dr. Peter Davies). Horseradish peroxidase-labeled conformation-sensitive secondary anti-mouse IgG for IP or anti-rabbit VeriBlot for IP Detection antibody (both at 1:20000; Abcam, Cambridge, MA) was detected by SuperSignal West Femto Maximum Sensitivity substrate (Thermo Fisher Scientific).

A dephosphorylation assay was performed using fresh-frozen brain tissue homogenized with a glass-Teflon homogenizer at 500 rpm in 10 volumes (wt/vol) of ice-cold lysis buffer containing 50 mM Tris, pH 7.8, 0.5 % NP40, 150 mM NaCl, and Halt protease inhibitor cocktail (Thermo Fisher Scientific, Waltham, MA). Samples were incubated on ice for 30 min, centrifuged at 1000 x g for 10 min, and supernatant was collected. Reaction mixtures (51 µul) consisted of 39 µl of supernatant, 1 µl of protease inhibitor cocktail, 5 µl of 10X NEBuffer for protein metallophosphatases, 5 µl of 10 mM $MnCl_2$, 1 µl of lambda protein phosphatase (New England BioLabs, Ipswich, MA). Each mixture was incubated at 30 °C for either 1, 2, 3, or 4 h. Additional 1 µl of lambda protein phosphatase and 1 µl of protease inhibitor cocktail were added in each mixture every hour.

Proximity ligation assay

A proximity ligation assay was performed on formalin-fixed paraffin embedded 5 µm-thick hippocampal sections mounted on charged slides using a Duolink kit (MilliporeSigma, St. Louis, MO). Sections were deparaffinized and incubated in sodium citrate buffer (10 mM sodium citrate, 0.05 % Tween 20, pH 6.0) at 95 °C for 20 min, washed in running water, incubated in 0.2 % Tween 20 in PBS at room temperature for 20 min, and washed in PBS 3 times for 5 minutes.. From blocking, assays were performed using the *in situ* red starter kit according to the manufacture's protocol with JADE1 antisera (1:20) and 0N tau antisera (1:500; BioLegend, San Diego, CA). Two control assays were also performed, one with JADE1 antisera only, and the other with anti-0N tau antisera. All samples were counterstained with 4′,6-diamidino-2-phenylindole (DAPI). Sections were imaged using an Axioview fluorescent microscope (Carl Zeiss, Oberkochen, Germany) and processed using Zen Blue software.

In vivo Drosophila *model*

Drosophila stocks, crosses, and aging were performed at 25 °C for the duration of the experiment and an equal number of male and female flies were used for each experiment. The GAL4-UAS expression system and the pan-neuronal elav-GAL4 driver were used to control transgenic human tau and rno expression. Analyses were run on four fly groups (Bloomington stock rno^{RNAi} line number 57774): elav-GAL4 driver in the heterozygous state (control, elav-GAL4/+), elav-Gal4 positive plus rno^{RNAi} positive group (control +

rno^{RNAi}, elav-GAL4/+;UAS-rno^{RNAi}/+), elav-Gal4 positive transgenic human UAS-tau^{R406W} tau group (0N4R Tau, elav-GAL4/+;UAS-Tau^{R406W}), elav-Gal4 positive human transgenic UAS-tau^{R406W} tau plus rno^{RNAi} positive group (0N4R Tau + rno^{RNAi}, elav-GAL4/+;UAS-Tau^{R406W}/UAS-rno^{RNAi}). An additional rno^{RNAi} lines were used but was did not produce progeny when crossed to tau transgenic *Drosophila,* as often occurs with strong enhancers (Bloomington stock rno^{RNAi} line number 62880). Flies were aged to 10 days, at which point terminal deoxynucleotidyl transferase dUTP nick end-labeling (TUNEL) assay was performed in the fly brain (*n*=6 per genotype) and a blinded assessment of the fly eye phenotype was performed (*n*=16 total). TUNEL was performed on 4 μm formalin-fixed paraffin-embedded fly heads. Quantification of TUNEL-positive nuclei was performed throughout the entire brain using DAB-based detection and bright field microscopy. Fly eye phenotype scoring was performed blindly using light microscopy (*n*=16). The blinded rater semi-quantitively evaluated the eye for four distinct qualities including roughness, size, shape and conical shape on a 1 to 5 scale (five being the most severe phenotype) and an average summary score was calculated.

Statistical analysis

For GWAS, statistical analysis was performed in PLINK and our genome wide significance value was $< 5 \times 10^{-8}$, which is Bonferroni-corrected for all the independent common SNPs across the human genome. Genome wide suggestive significant value was set at $< 5 \times 10^{-6}$. All other statistical analyses were performed in R. For non-normally distributed data a Wilcox test was used to test for significance, and an ANOVA was used for normally distributed data.

Results

We assembled the first cohort of individuals with primary age-related tauopathy (PART) in which all individuals were neuropathologically confirmed to be devoid of any neuritic plaques. Autopsy brain tissue samples (*n*=647) were obtained from 21 brain banks. While each center had performed a comprehensive neurodegeneration workup, we restained and reassessed these cases for PART pathology as a component of our ongoing histological studies[40]. Neurofibrillary tangles (NFTs) were assessed using the Braak staging system which ranged from 0-IV with all stages well represented, as is consistent with PART (Table 1). The average age of death was 83 years old, and the number of male and females in the study was approximately equal. Amongst the assigned Braak stages, stage II had the highest abundance (*n*=189), relatively equal amounts in stages III (*n*=152) and I, (*n*=142), and the lowest in stages 0 (n=71) and IV (*n*=93). Sixty-six percent of the cases were cognitively normal, however amongst stages I-IV, there was an equal number of cognitively impaired individuals. Braak staging performed at each center was not disproportionally skewed (Supplementary Fig. 1a). Lastly, we investigated the effect of age of death on Braak stage with respect to cognitive status and found a positive correlation that does not significantly change when cognitive status is accounted for in the model (Supplementary Fig. 1a,b). In summary, our cohort consists of primarily older individuals, with a range of clinical cognitive symptoms, as well as a broad spectrum of regional tau distribution, demonstrating the diversity of both the clinical and neuropathological features of the condition.

Table 1 | Subject data stratified by Braak stage

Braak NFT stage	n	Average age (range)	Male (%) / Female (%)	Normal (%) / MCI (%) / Dementia (%)*
0 (71)	**71**	71.2 (51-104)	48 (7.5) / 23 (3.5)	58 (8.9) / 7 (1.0) / 6 (0.9)
I (142)	**142**	78.1 (53-108)	88 (13.6) / 54 (8.3)	99 (15.3) / 17 (2.6) / 22 (3.4)
II (189)	**189**	84.1 (51-107)	98 (15.1) / 91 (14.0)	126 (19.4) / 40 (6.1) / 21 (3.2)
III (152)	**152**	88.8 (68-105)	59 (9.1) / 93 (14.8)	96 (14.8) / 29 (4.4) / 26 (4.0)
IV (93)	**93**	91.2 (67-106)	29 (4.4) / 64 (9.8)	50 (7.7) / 22 (3.4) / 21 (3.2)
Total (647)	**647**	83.5 (51-108)	322 (49.7) / 325 (50.2)	429 (66.3) / 115 (17.7) / 96 (14.8)

*7 samples did not have cognative status available, MCI = mild cognitive impairment

Using this cohort, we ran a quantitative trait association analysis across the entire genome to identify novel genetic risk loci in PART. Using Braak stage as a quantitative trait revealed a genome wide associated signal on chromosome 4q28.2 (Fig. 1a, rs56405341; linear regression β=0.35, standard error=0.06, $p=4.82 \times 10^{-8}$) and suggestive signals in 14 other loci (Table 2 and Supplementary Table 3). Our model, which adjusted for age, sex, and genotyping platform and principal component 1-4 produced a λ of

1.04 (Supplementary Fig. 2a). The genome wide significant variant (rs56405341) has a minor allele frequency of 0.27. The locusZoom plot indicates our significant SNP is not directly in an intron of any specific gene, but near *C4orf33*, *SCLT1* and *JADE1* (Figure 1b). We also observed in our regional plot that the lead SNP has a total of 22 other SNPs in Linkage Disequilibrium (r^2 > 0.8, Supplementary table 4). Further examination of the homozygous and heterozygous alleles using strip chart shows the significant relationship between higher Braak stage and homozygous minor allele carriers (Figure 1 c, AA-AG p=0.024, AA-GG p=3.3 × 10^{-5}, AG-GG p=7.2 × 10^{-5}). Separate analyses two different genotyping chip validated our findings by showing replication of the signal on each genotyping platform, as well as comparable lambda values (Infinium OmniExpress-24, n=440, β=0.27, SE=0.05, p=1.11× 10^{-6}, λ = 1.03, Global screening array β=0.20, SE=0.08, p=1.42× 10^{-2}, λ = 1.01, Supplementary Table 2 and Fig. 5 a-d). The individual summary statistics derived from the separate chip analysis were then combined to run a meta-analysis, and the resulting p-value was similar to value on the combined analysis, as well as agreement in the direction of effect tested allele (p=5.61 × 10^{-8}).

Table 2 | Summary of SNPs reaching genome-wide suggestive and significance

Chr	Base pair	SNP	Genes	A1	Beta	SE	L95	U95	t-statistic	*p*
2	11935322	rs78580932	GREB1, NTSR2, LPIN1, MIR4262	C	-0.54	0.10	-0.76	-0.34	-5.15	3.55E-07
2	235768810	rs74600760	ARL4C, SH3BP4	T	-0.53	0.11	-0.74	-0.32	-4.86	1.48E-06
3	61518166	rs111610564	FHIT, PTPRG	C	-0.49	0.10	-0.70	-0.30	-4.82	1.81E-06
3	140216029	rs349509	CLSTN2, CLSTN2-AS1, TRIM42	A	-0.77	0.16	-1.08	-0.47	-4.97	8.64E-07
3	179019705	rs13323081	PIK3CA, KCNMB3, ZNF639, MFN1	G	0.24	0.05	0.15	0.33	5.17	3.16E-07
4	130085480	rs56405341	C4orf33, SCLT1, JADE1	A	0.25	0.05	0.16	0.35	5.52	**4.82E-08**
4	137329297	rs77506227	-	A	-0.79	0.16	-1.12	-0.48	-4.88	1.34E-06
5	150473104	rs6579838	GPX3, TNIP1, ANXA6	C	0.23	0.05	0.14	0.32	5.10	4.57E-07
10	124487608	rs150945906	DMBT1, C10orf120, DMBT1P1	A	-0.64	0.14	-0.91	-0.38	-4.77	2.31E-06
15	24515682	rs147462127	PWRN2, PWRN1	T	-0.84	0.17	-1.18	-0.51	-4.98	8.37E-07
15	36865219	rs185845364	C15orf41, CSNK1A1P1	G	-0.79	0.16	-1.11	-0.48	-4.94	9.79E-07
17	1879293	rs12946465	RPA1, RTN4RL1, DPH1, OVCA2	C	-0.21	0.05	-0.31	-0.13	-4.75	2.51E-06
19	45719790	rs10415392	TRAPPC6A, BLOC1S3, EXO3L2, MARK4	T	0.34	0.07	0.21	0.48	4.85	1.59E-06
20	56754110	rs78923929	C20orf85, PPP4R1L, RAB22A	A	-0.65	0.13	-0.92	-0.40	-4.95	9.76E-07

genome wide significant difference in bold, chr=chromosome. SNP=single nucleotide polymorphism, SE=standard error

Replication of our SNP in an independent cohort proved challenging given the lack of datasets containing similarly neuropathologically ascertained individuals with PART. Nevertheless, we identified two other SNPs (rs4975209 and rs10009321) in the 4q28.2 locus in a prior Alzheimer disease (AD) GWAS that also used Braak as a quantitative trait, however they were not in high D' with rs56405341, our lead SNP [52]. We also observed in a separate AD GWAS using the cerebral spinal fluid Aβ42/40 ratio (dichotomized normal and abnormal) another SNP in the region (rs13129839) in high D' with our lead and supporting SNPs (>0.89), at a genome-wide suggestive significance level and with a positive (protective) odds ratio (*p*

= 9.0 × 10^{-6}, OR = 0.043) [53]. Taken together, these two independent genetic studies in AD suggest the signal in our GWAS might not be spurious.

We also examined candidate SNPs previously found to be associated with AD and progressive supranuclear palsy (PSP) in prior GWAS studies to explore convergent and divergent genetic risk (Table 3, Supplementary table 5). Of the 52 candidates investigated, we found five associated with PART (*SLC24A4, MS4A6A, HS3ST1, MAPT,* and *EIF2AK3*). rs12590654, which is associated with *SLC24A4*, had the highest significance level (*p*=0.001). rs1582763, rs2081545, rs7935829, were all associated with *MS4A6A* (*p*=0.01, 0.01, 0.02 respectively). The remaining AD SNP, rs7657553, was associated with *HS3ST1* (*p*=0.02). We found two variants that overlapped with PSP risk. rs242557 (*p*=0.02) in the *MAPT* locus, and rs7571971 (*p*=0.03) in the *EIF2AK3* locus. In summary, seven of the 52 probed risk AD and PSP SNPs showed significant associations (*p*<0.05) in PART.

Table 3 | Signficant overlapping PART genetic hits with Alzheimer disease and progressive supranuclear palsy

Associated disease	Chr	Base pair	SNP	Gene	A1	Beta	SE	L95	U95	t-statistic	*p*
AD	14	92938855	rs12590654	SLC24A4	A	-0.14	0.044	-0.23	-0.05	-3.19	0.0015
AD	11	60021948	rs1582763	MS4A6A	A	-0.11	0.044	-0.19	-0.02	-2.47	0.0138
AD	11	59958380	rs2081545	MS4A6A	A	-0.10	0.044	-0.19	-0.02	-2.36	0.0185
AD	4	11723235	rs7657553	HS3ST1	A	0.11	0.048	0.01	0.20	2.24	0.0255
PSP	17	44019712	rs242557	MAPT	A	0.10	0.047	0.01	0.20	2.24	0.0256
AD	11	59942815	rs7935829	MS4A6A	G	-0.10	0.043	-0.18	-0.01	-2.21	0.0274
PSP	2	88895351	rs7571971	EIF2AK3	T	-0.10	0.047	-0.19	-0.01	-2.09	0.0373

AD= Alzheimer disease, PSP=progressive supranuclear palsy, Chr=chromosome, SNP=single nucleotide polymorphism

Next, we refocused on our strongest association at the 4q28.2 locus. Examination of RNA expression quantitative trait loci (eQTL) using the Brain-eMeta eQTL summary data (derived from six datasets; Genotype-Tissue Expression v6, the CommonMind Consortium, Religious Orders Study and Memory and Aging Project, the Brain eQTL Almanac project, the Architecture of Gene Expression, and eQTLGen) did not contain significant SNP associated eQTLs for any of the genes in the 4q28.2 locus [54]. Because our GWAS quantitative trait was specific to tau pathology, we then examined mRNA expression levels of all the genes contained in the locus using a novel single-cell soma RNA sequencing dataset which measured transcriptomic changes specifically in tangle-bearing neurons and non-tangle-bearing neurons (Fig. 2a-c). Using this dataset, we found that tangle-bearing excitatory neurons significantly differentially expressed *JADE1* compared to non-tangle-bearing excitatory neurons (*p*=1.04×10^{-61}). Conversely *C4orf33* and *SCLT1* had low levels of expression regardless of cell type and tangle status. Additionally, we observed an upregulation of *JADE1* expression in tangle-bearing inhibitory neurons however it was statistically

underpowered due to low cell abundance and high variance. Furthermore, we observed two subpopulations of excitatory neurons in which *JADE1* was significantly differentially expressed (adjusted p=4.55×10^{-15}, 7.82×10^{-8}). We then examined the relative average expression and percentage of cells expressing *JADE1* and observed increases in both metrics in tangle-containing neuronal populations compared to non-tangle-containing neuronal populations (Fig. 2d-f). *SCLT1* and *C4orf33* had nominal expression levels in a substantially smaller percentage of neurons. Taken together, these data suggest increased *JADE1* expression is unique to specific populations of neurons which also contain NFTs. Because we did not observe significant differences in *C4orf33* or *SCLT1* expression across the two groups, and the signals were very low, these data suggest that *JADE1* as the strongest candidate gene in the locus.

Given our evidence that *JADE1* is genetically and transcriptionally associated with NFT pathology, we conducted an immunohistochemical study using specific antisera to JADE1 in our collection of post-mortem tauopathy brain tissue (Fig. 3). We assessed tauopathies that are known to involve preferentially tau isoforms with 3 microtubule-binding domain repeats (3R), 4 microtubule-binding domain repeats (4R) or a mixture of the two. We found strong and specific JADE1 immunopositivity in structures morphologically indicative of mature aggregate containing intracellular NFT in not only PART, but also the other mixed 3R/4R tauopathies (i.e., AD and chronic traumatic encephalopathy, Fig 3a-f). NFT pathology in PSP, corticobasal degeneration (CBD), and argyrophilic grain disease (AGD) were also immunopositive for JADE1 (Fig. 3g-l). Notably, gliofibrillary pathology in these diseases (i.e., aging-related tau astrogliopathy, tufted astrocytes, and astroglial plaques) were also immunopositive. Surprisingly, no signal was detected in NFT in Pick disease (PiD), a predominately 3R tauopathy (Fig. 3m,n). Double labeling experiments showed that early pre-NFT were negative for JADE1 suggesting that this factor begins to coalesce into NFT at the transition to the aggregate stage (Fig. 3o). To ensure the antibody was specifically targeting the JADE1 peptide and not binding non-specifically to NFT pathology, we blocked the JADE1 antibody and did not observe any staining in neurons that had the morphological features of an NFT (Fig. 3p). These findings indicate that JADE1 protein expression is localized specifically to cells with mature NFTs. Furthermore, JADE1 upregulation does not occur in PiD, the only 3R tauopathy examined, suggesting isoform specificity of expression.

We then biochemically examined protein expression of JADE1 by western blotting using crude lysates derived from the entorhinal cortex and hippocampus proper (cornu ammonis 1-4 and dentate gyrus) of PART and AD individuals. JADE1 exists as 2 isoforms, JADE1 long (JADE1L) and JADE1 short (JADE1S), both of which contain proline, glutamic acid, serine, threonine (PEST) domains and 2 PHD fingers. However, the long form is 333 amino acid sequences greater in length and contains an additional PEST domain as well as a nuclear localization signal (Fig 4a). A Western blot analysis revealed a strong signal in both brain regions and diseases for JADE1S, but no bands were observed in the expected weight for JADE1L, indicating the observed signal is specific to the short isoform of JADE1 (Fig. 4b). This signal is in agreement with the immunohistochemical data given we did not observe a nuclear JADE1 signal which would suggest JADE1L, the form containing the nuclear localization signal, was also expressed. Furthermore, cytoplasmic colocalization of JADE1 and NFTs immunohistochemically raises a possibility that they form a functional complex in tauopathy brains. To examine this, co-immunoprecipitation (IP) was performed using crude brain lysate from PART individuals as the input. We first IPed using JADE1 antisera and observed a banding pattern that suggests JADE1 pulls down tau near the molecular weight of the 0N4R isoform (Fig. 4 c). To confirm these results, we reverse co-IPed JADE1 with 0N tau antisera and observed a banding pattern indicating the JADE1S isoform was pulled down (Fig. 4d). To investigate the observed JADE1 immunoprecipitated lower banding pattern (Fig. 4c), we treated this form with protein phosphatase over time and observed a shift over time to the expected 58 kDa weight (Fig. 4e), indicating JADE1 anti-sera was not able to recognize the more abundant native phosphorylated JADE1S and instead a low abundant species of the protein. This data suggests the predominant form of the JADE1S input is likely being biologically modified (i.e., phosphorylation, acetylation, etc.). Staining with C-terminal isoform-specific anti-tau antibodies (3R and 4R tau) revealed that the co-immunoprecipitated tau was predominantly 4R, thus 0N4R tau (Fig. 4f,g). We then ran western blots for the IPed JADE1 using multiple phospho-tau site-specific antibodies including RZ3 (pThr231), PHF1 (pThr181), CP13 (Ser202), AT8 (Ser202, pThr205), S214 (Ser214) and PG5 (Ser409) of which multiple phosphor tau epitopes showed prominent reactivity (Fig. 4h). Lastly, to confirm protein-protein interactions of Jade1S and 0N tau, proximity-ligation assays (PLA) were performed in fixed hippocampus from PART individuals. The PLA technique utilizes one pair of oligonucleotide-labeled antibodies that detects different epitopes of the two proteins in close proximity

(maximum 30-40 nm apart). The prominent red fluorescence signal surrounding the nuclei of a neuron indicates the close proximity of these two proteins (Fig. 4i), whereas control samples lacking one of the two antisera did not show any signal (Supplementary Fig. 7e,f). In summary, the biochemical data strongly indicates a JADE1S, 0N4R tau immunocomplex.

Lastly, we asked whether JADE1 plays a functional role in tau-induced neurotoxicity. We used a *Drosophila* model that overexpresses human mutant 0N4R tau[55] as well as RNAi-mediated reduction of rhinoceros (rno), the highest matched JADE1 human ortholog in *Drosophila*. We first blindly evaluated the fly eye phenotype using a semi-quantitative assessment of eye size, roughness, overall shape, and conical shape and saw a significant increase in eye severity between tau transgenic *Drosophila* and tau transgenic *Drosophila* with rno knockdown (Fig. 5a-e, $p=8.7 \times 10^{-5}$). We did not observe significant differences between rno^{rnai} and control group in the absence of transgenic tau. To directly quantify neurodegeneration in the *Drosophila* brain, we quantified TUNEL-positive cells throughout the *Drosophila* brain. We find that rno knockdown significantly enhances neurotoxicity in tau transgenic *Drosophila* but is not sufficient to induce neurotoxicity in control flies based on TUNEL staining ($p=0.008$, Fig. 5f-i). These data provide *in vivo* evidence that JADE1/rno loss plays a mechanistic role in promoting neurotoxicity in tauopathy, and suggest that proper functioning of JADE1/rno is protective

Discussion

Genome-wide association studies (GWAS) have enabled advances in our understanding of sporadic tauopathies [19,56-61]. Yet, in the context of the growing numbers of genes associated with Alzheimer disease (AD) [32], direct links with tau proteinopathy have been challenging to pinpoint as association signals show minimal overlap with factors classically implicated in tauopathy (e.g., proteostasis, tau protein kinases, etc.). This is not surprising given the ubiquity and heterogeneity of tau and other pathological changes in the aging human brain that are variably associated with cognitive impairment, which is the phenotype in most genetic studies despite the fact that it is a non-specific trait. We performed an autopsy-based GWAS, which minimizes classification errors and other issues with clinical studies of dementia, assembling the largest cohort of post-mortem brain tissues from aged individuals devoid of amyloid pathology with a goal of identifying factors independently associated with primary age-related tauopathy (PART). In doing so, we sought to provide genetic evidence that might clarify the controversial relationship between PART and AD, which it closely resembles neuropathologically. We failed to find an association with *APOE* ε4, the strongest common risk allele for sporadic late-onset AD. We did, however, find associations with other candidate loci in AD and progressive supranuclear palsy (*SLC24A4*, *MS4A6A*, *HS3ST1*, *MAPT* and *EIF2AK3*), as well as a novel genome-wide significant association at the chromosome 4q28.2 locus. Our data indicate that among genes in this locus, only the gene for apoptosis and differentiation in epithelia 1 (*JADE1*), a member of a small protein family that serves as a multifunctional adaptor implicated in renal and other cancers[62-64], is upregulated in tangle-bearing neurons on both the mRNA and protein levels. This accumulation of JADE1 protein in NFT is not specific to PART but occurs in AD and all tauopathies with accumulation of 4R isoforms, but not in Pick disease which is a 3R tauopathy, indicating that this is generally a shared feature. We also show that JADE1 binds 0N4R tau, an isoform proposed to be a critical driver of tau pathology[65,66]. Finally, experiments in *Drosophila* show that reducing expression of the *JADE1* homolog rhinoceros (rno) exacerbates tau-induced neurotoxicity *in vivo*. Together, these findings strongly argue that JADE1 is a factor broadly capable of protecting neurons from neurofibrillary cell death that links PART to the tauopathic component of AD.

We confirm that the genetics of PART has a partial overlap with sporadic late-onset AD and replicated the consistent finding showing the lack of a signal in the *APOE* locus despite its strong

association with AD [32,67-70]. It has been shown previously that PART individuals have a higher *APOE* □2 allele frequency which distinguishes PART neuropathologically and genetically from AD [71-73]. We have reported the frequency of the *APOE* ε4 allele is lower in PART[28] and other studies have revealed similar findings in independent cohorts [6,33]. It should be noted that these values can fail to reach significance when cross comparing groups with varying degrees of neuritic plaque pathology [33,74]. Recent studies in mice and humans have indicated that the *APOE* ε4 allele may exacerbate tau pathology independently of Aβ plaques[75], however other human studies failed to show an interaction[76,77]. These results add to the strong evidence that PART is entirely independent of *APOE* ε4 regardless of amyloid plaque pathology.

17q21.31 *MAPT* locus is the strongest genetic risk factor for PSP [26], which we and others had previously reported is also associated with PART [28,31]. The *MAPT* H1 haplotype has also been associated with AD [78-80], however this region has a complex haplotype structure and may be more important in specific AD subgroups given the modest signal and variable findings in these association studies[81,82]. Intriguingly, in one AD GWAS using clinically ascertained individuals, removal of *APOE* ε4 carriers enhanced signals in the 17q21.31 locus [23]. In the present study, there was only a modest association of *MAPT* with PART. This result may stem from differences in cohort selection with previous studies focusing on extremes, while we included a range of pathological severity, especially mildly affected individuals. Together, these data highlight that further investigation of the role of 17q21.31 *MAPT* locus in PART is warranted.

With regards to genes other than *APOE* and *MAPT*, we found four additional association signals in PART that overlap with either AD or PSP. Eukaryotic translation initiation factor 2 alpha kinase 3 (*EIF2AK3*) encodes an endoplasmic reticulum (ER) membrane protein critical for the unfolded protein response (UPR)[83,84]. Activation of the UPR has been observed and positively correlated with tau pathology, but not with Aβ plaque burden, in the hippocampus of aged cognitively normal individuals [83]. Solute carrier family 24 member 4 (*SLC24A4*), a gene in the locus most strongly associated with PART and AD, is a member of the potassium-dependent sodium/calcium exchanger protein family and is involved in neural development, however little is known about its possible function in AD [85,86]. Additionally, we identified an association of PART with the membrane spanning 4-domains A6A (*MS4A6A*) locus, which contains the binding regions for the transcription factor PU.1 which is selectively expressed in brain microglia and macrophages [87]. The last overlapping genetic locus that contains heparan sulfate-glucosamine 3-sulfotransferase 1 (HS3ST1), has

been suggested to modulate heparan sulfate proteoglycans as receptors for the spreading of tau [88,89]. Taken together, these data are compatible with the hypothesis that the genes we identified in our GWAS are possible modulators of tau pathology.

Our study highlighted a novel locus on chromosome 4q28.2, that previously gave a suggestive signal in an independent autopsy GWAS in AD that also used Braak NFT stage as an endophenotype and a second GWAS focusing on dichotomized CSF Aβ positivity[53,90]. This prompted us to focus on this locus for further validation and functional studies. Because we failed to identify expression quantitative trait locus in both blood and brain datasets, we hypothesized that given our trait was tangle-specific, modulation of mRNA expression of genes in the locus might also be cell-type specific. This hypothesis was also motivated by the increase in genetic to transcriptomic associations found in cell specific populations in other contexts [91-93]. Our results indicate that of the genes in the 4q28.2 locus, only *JADE1* mRNA was significantly and differently expressed in tangle-bearing neurons. Our immunohistochemical studies also showed JADE1 protein accumulation in both neuronal and glial tangle containing cells, validating these findings. Thus, JADE1 is most likely responsible for the GWAS signal at this locus.

Our immunohistochemical studies indicate that *JADE1* is potentially involved broadly in tauopathies. We observed immunopositivity not only in PART tangles, but also in tauopathies with aggregates containing 4R tau and mixed tauopathies with aggregates containing both 3R and 4R. The absence of staining in Pick disease, the only tauopathy with 3R tau aggregates examined, was surprising. Our biochemical studies suggest that JADE1 protein specifically interacts with 0N4R tau that is phosphorylated on epitopes known to be hyperphosphorylated in NFT. Our proximity ligation assay confirms the direct interaction between JADE1 protein and tau. Studies using cryo-EM and mass spectrometry have shown the ultrastructure of tau aggregates at unprecedented resolution, and it has been reported that 0N4R has a unique single β-sheet conformation for the fibril core [94-96]. Intriguingly, recent mass spectrometry profiling studies of human postmortem brain tissues have suggested that changes in 0N4R tau isoform specifically is an early event in tauopathy [97]. Double labeling experiments indicate that JADE1 increases shortly after the pre-tangle stage, accumulating alongside insoluble tau aggregates during the transition to the intercellular tangle stage perhaps reflecting a reactive/protective compensatory role [98].

Our findings provide important clues as to how *JADE1* may be functioning in tauopathy. *JADE1* has been previously implicated as a renal tumor suppressor involved in apoptosis, well as inhibition of Wnt signaling by ubiquitylating β-catenin, and interactions with cell-cycle regulators [62,99-103]. Of the two JADE1 isoforms, only the short form which lacks a nuclear localization signal was observed, which was consistent with the cytoplasmic localization of the protein we observed by immunohistochemistry. This prompted us to hypothesize that JADE1S functions in the cytoplasm to mediate tauopathy. Our *in vivo* studies in which we reduced rno (the closest JADE1 ortholog) levels in *Drosophila* overexpressing mutant human 0N4R tau significantly enhanced the tau-induced rough eye phenotype as well as TUNEL-positive cells, a marker of apoptotic DNA fragmentation. While JADE1 has been shown to promote apoptosis in some contexts, our RNAi knockdown experiments suggest that proper functioning of JADE1 may be neuroprotective. Consistent with this, other studies have demonstrated that loss of rno function attenuates apoptosis in *Drosophila*[104]. Because previous studies have found JADE1 to be stabilized by the von Hippel-Lindau tumor suppressor which is a component of an E3 ubiquitin-protein ligase activity, JADE1 may be working with 0N4R tau through a similar mechanism to promote ubiquitin-mediated clearance of tau [105-107].

Our study has several notable limitations. Our sample size is small for GWAS standards; however, it should be noted that it is still the largest study of its kind. Given that PART is currently only reliably diagnosed postmortem, the study is limited by the availability of tissue that meet our strict criteria. Our study also relies on neuropathological assessments performed at multiple centers that may cause batch effects. While Braak staging is highly reproducible, with one report showing that across brains and raters the kappa score was greater than 0.90 [108], it is a semiquantitative (ordinal) variable. Further studies using a more quantitative approach to measuring tau burden that we have shown more closely align with functional clinical measures in PART may reveal additional candidates [109]. Additional follow-up studies in experimental models are necessary further to validate our findings.

In conclusion, therapies for AD in clinical trials are moving towards targeting tau due to the lack of clinical efficacy of Aβ modulating therapeutic approaches [110]. Here, by focusing on individuals with PART who lack Aβ plaques, we enriched our cohort for signals related to tau proteinopathy. Our analysis provides additional evidence that PART overlaps with but has considerable differences from AD. This interdisciplinary approach led to the identification of *JADE1*, which interacts with 0N4R tau, and is protective

in vivo. Thus, JADE1 is a potential novel biomarker that differentiates tauopathies. Further understanding the genetics of PART will provide pathways for rationally designed therapeutics for degenerative tauopathies.

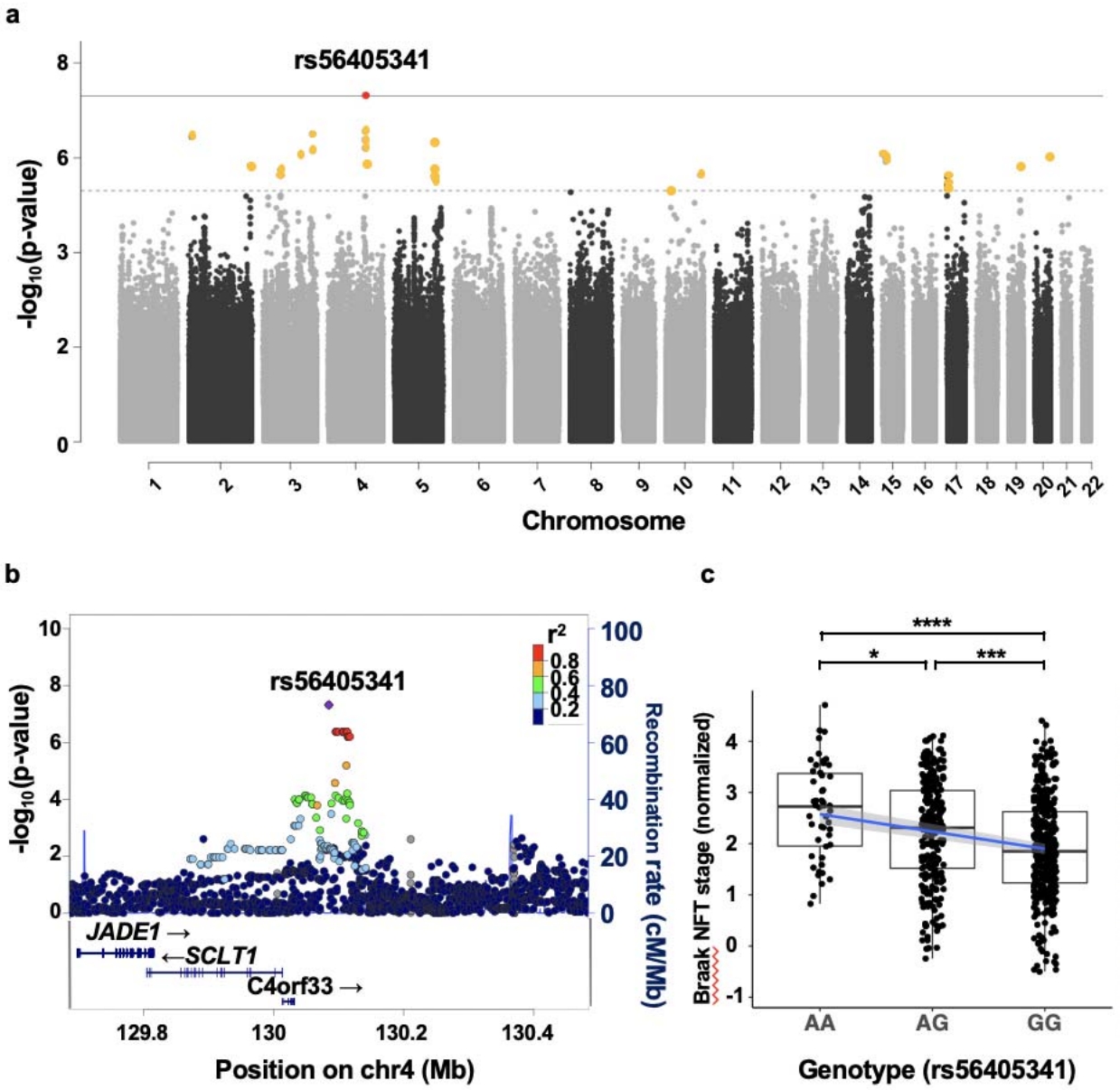

Fig. 1 | Genome-wide association study (GWAS) in primary age-related tauopathy. (**a**) A quantitative trait GWAS was performed using normalized Braak neurofibrillary tangle stage with age, sex, principle components (PCs) and genotyping SNP array as covariates (n=647). The threshold for genome-wide significance ($p<5 \times 10^{-8}$) is indicated by the solid grey line; the suggestive line ($p<5 \times 10^{-6}$) is indicated by the dotted line. (**b**) A LocusZoom plot shows a strong signal with multiple SNPs in LD on chromosome 4q28.2. The x-axis is the base pair position and the y axis is the $-\log_{10}$ of the p-value for the association with Braak stage. The blue line represents the recombination rate. (**c**) Association between single-nucleotide polymorphism (SNP), rs56405341 and Braak tangle stage (adjusted for age and sex). Pairwise comparisons using Wilcoxon rank sum test, AA-AG p=0.024, AA-GG p=3.3E-05, AG-GG p=7.2E-05.

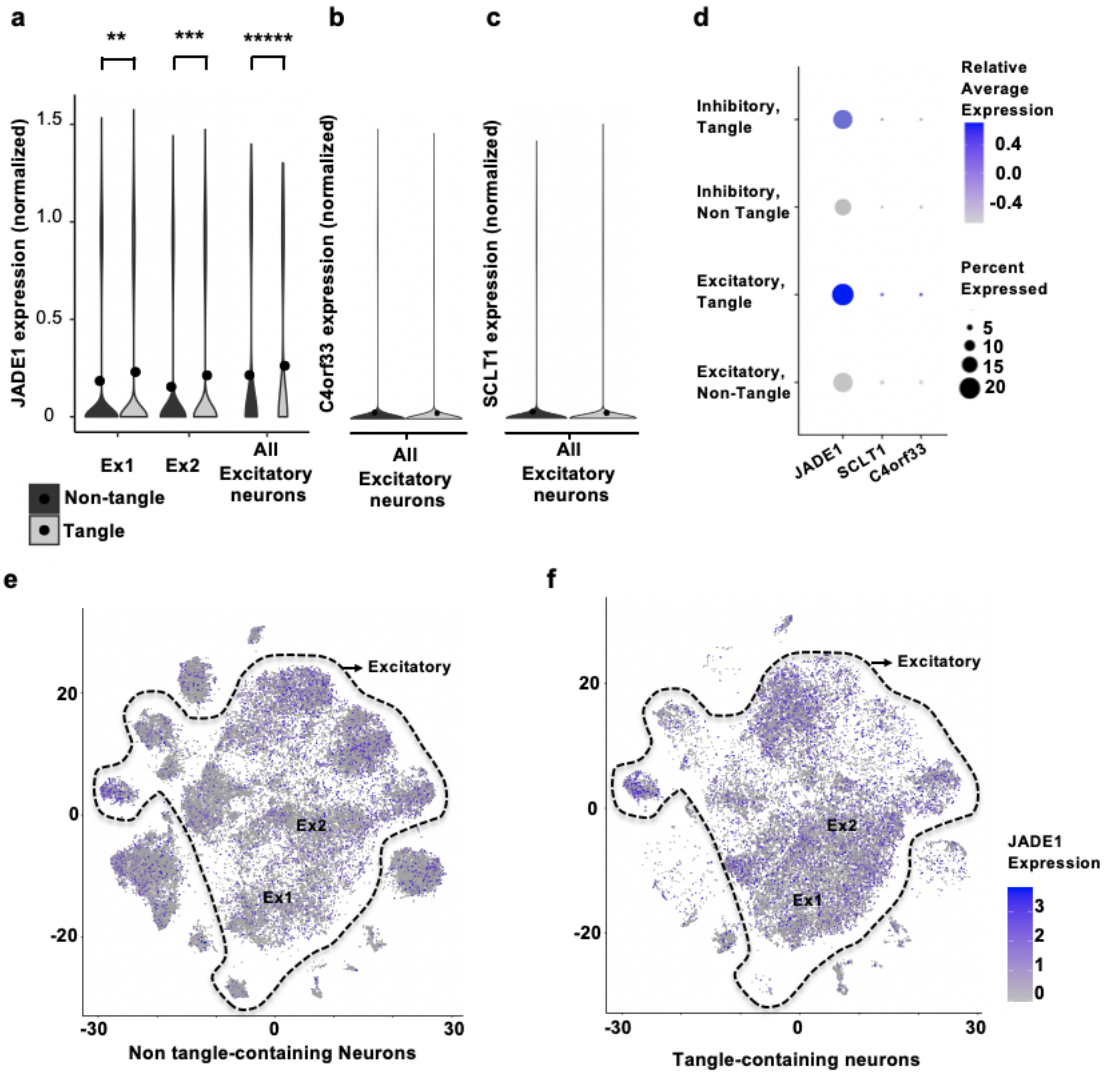

Fig. 2 | Single-cell sequencing of neurons with and without tau aggregates reveals *JADE1* mRNA is upregulated in tangle-bearing neurons. Neurons with and without neurofibrillary tangles from human post-mortem brains samples were separated using fluorescence-activated cell sorting and single-cell RNA-sequencing was performed. (**a**) In 2 unique excitatory neuronal populations *JADE1* mRNA was significantly differentially expressed in the tangle bearing neurons (adjusted p= 7.82×10^{-8}, 4.55×10^{-15}) and comparing the overall population of tangle-bearing excitatory neurons to non-tangle bearing neurons the value is highly significant (adjusted p=1.04×10^{-61}). (**b**,**c**) The other two genes in the locus, *C4orf33* and *SCLT1*, were overall nominally expressed in both excitatory neuronal groups, as well as subclusters (data not shown). (**d**) A dot plot showing average relative expression and percent expression of the candidate genes in the locus. Both *JADE1* relative average expression and percentage of cells expressed was higher than *C4orf33* and *SCLT1*. (**e**,**f**) A t-distributed stochastic neighbor embedding (tSNE) plot showing the populations of neurons, tangle bearing status, and relative expression of *JADE1* in neuronal subpopulations.

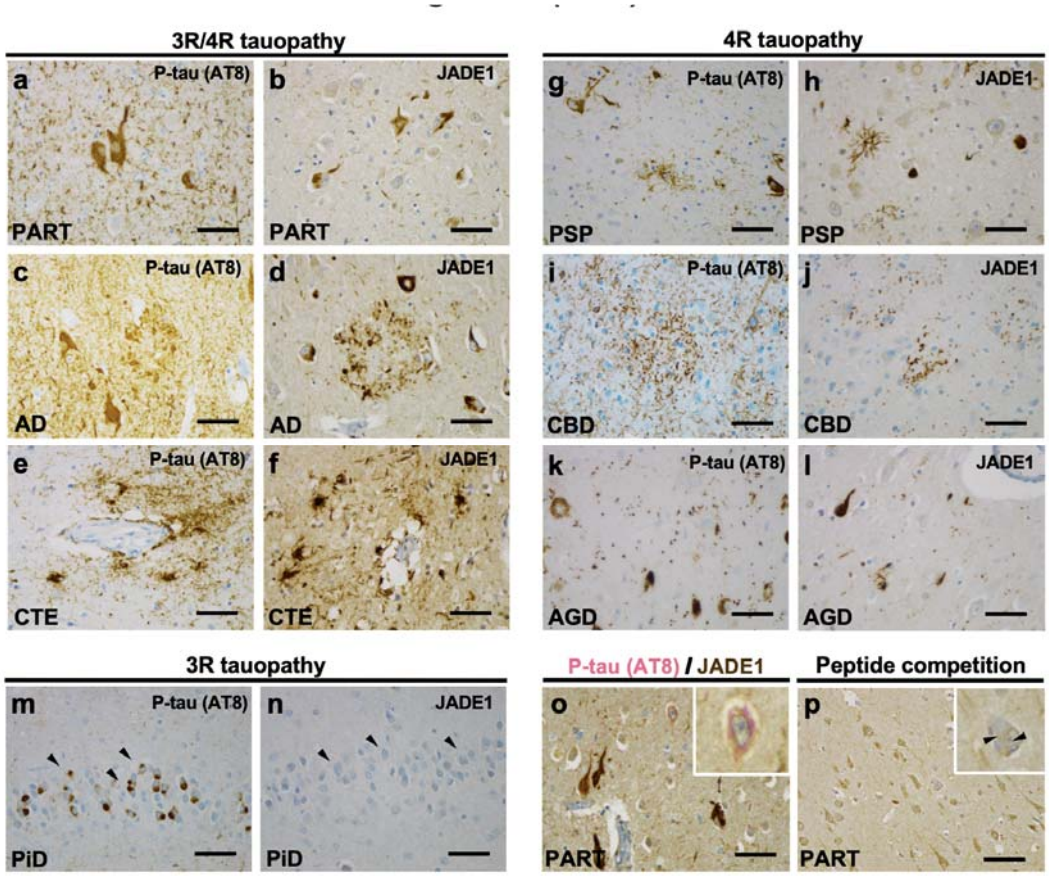

Fig. 3 | Selective immunolabeling of tau aggregates containing tau with four microtubule-binding domain repeats (4R), but not three (3R), in post-mortem human tauopathy brains with antisera targeting JADE1 protein. Immunohistochemical staining with phospho-tau (p-tau) specific antisera (AT8) and JADE1 specific antisera demonstrates neurofibrillary tangles (NFT) formation marked by the presence of JADE1 is specific populations of neurons and glia. (**a,b**) Primary age-related tauopathy (PART, *n*=3) NFTs contain JADE1 positive staining in the soma and neurites in the entorhinal cortex. (**c,d**) Alzheimer disease (AD, *n*=3) individual with beta-amyloid AT8-positive neuritic plaques and NFTs in the subiculum also display JADE1 immunopositivity in dystrophic neurites and NFTs. (**e,f**) Chronic traumatic encephalopathy (CTE, *n*=3) contains positive p-tau staining around a blood vessel in the depth of a neocortical sulcus that is also immunopositive for JADE1. (**g,h**) AT8 positive tufted astrocytes, oligodendroglial coiled bodies, and NFTs are positive in the subthalamic nucleus in a individual with progressive supranuclear palsy (PSP, *n*=3) which are also in immunopositive for JADE1**.** (**i,j**) Astrocytic plaques in corticobasal degeneration (CBD, *n*=3) and extensive thread-like pathology positive for p-tau and JADE1 in the neocortex. (**k,l**) In the cornu ammonis 1 (CA1) sector in a individual with argyrophilic grain disease (AGD, *n*=3), abundant grains that are immunopositive for p-tau and JADE1 are evident. (**m,n**) Pick disease (PiD), a 3R tauopathy, with Pick bodies in the dentate gyrus that are immunopositive for p-tau but negative for JADE1. (**o)** Double staining of a PART entorhinal cortex showing the absence of JADE1 (brown) staining in early pre-tangles, but the presence of p-tau (pink, see inset). (**p**) peptide competition demonstrating the antisera for JADE1 is specifically binding to the correct epitope give then absence of positive staining, but the presence of a tangle (inset). Scale bar 100 µm.

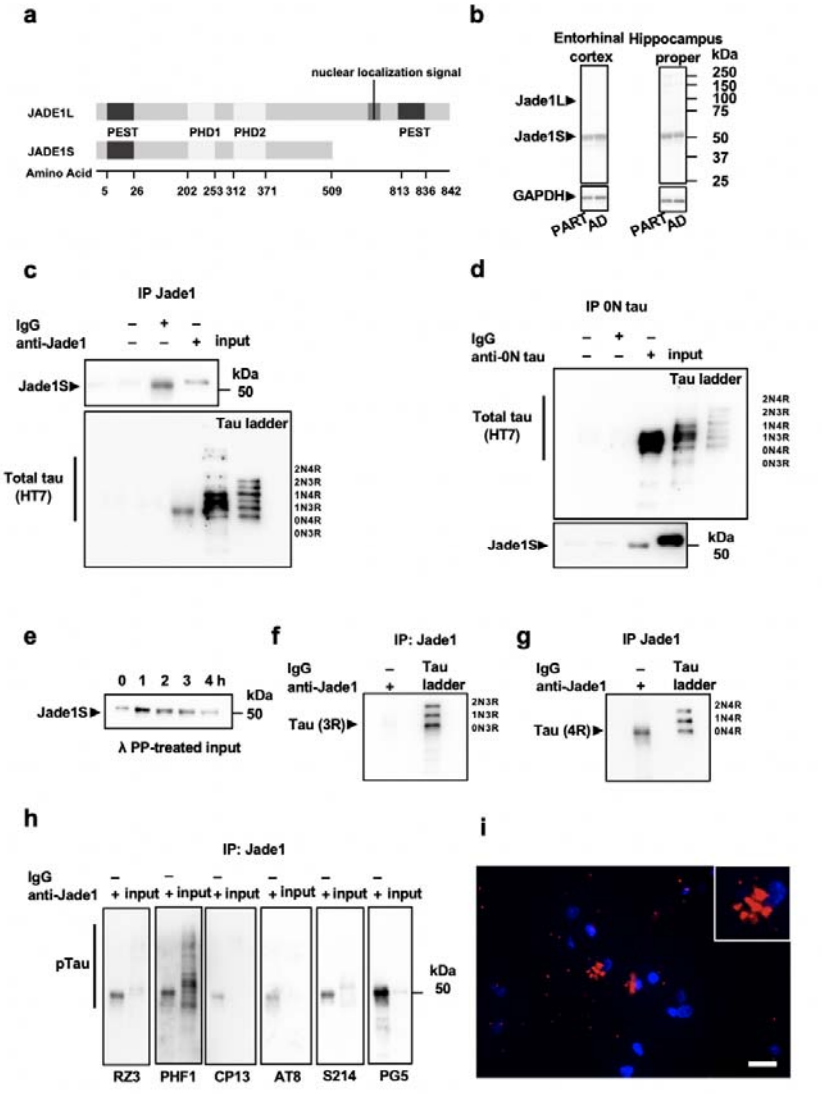

Fig. 4. | Biochemical analysis of JADE1S and total tau validates the interaction with 4 microtubule-binding domain repeats (4R) but not 3R in post-mortem human brain tissue from tauopathy individuals

(**a**) Schematic of the two JADE1 isoforms, JADE1S and JADE1L (**b**) Representative immunoblot using antisera targeting JADE1 measured in entorhinal cortex and cornu ammonis in individuals with primary age-related tauopathy (PART) and Alzheimer disease (AD) shows a banding pattern with the JADE1S isoform at 58 kDa but not the JADE1L at 95 kDA. GAPDH was used as a loading standard. (**c**) Co-immunoprecipitation (co-IP) using JADE1 antisera pulls down tau near the molecular weight of the 0N4R isoform. (**d**) Reverse co-IP with 0N tau antisera pulls down the JADE1S isoform. (**e)** The pulled down form of Jade1S molecular weight shifts downward after treatment with lambda protein phosphatase over time to expected 58 kDa weight. (**f,g**) Co-IPed tau with JADE1 stained with C-terminal isoform specific anti-tau antisera are the 0N4R isoform and not the 3R isoform (**h**) Co-immunoprecipitated tau was positively stained with multiple phospho-tau specific antibodies with the largest signal coming from pSer396 pSer404 (PHF1), pSer214 (S214), and pSer409 (PG5). (**i)** Duo-link assay showing positive luorescence signal (red) around the nucleus of neurons (blue) indicating the potential interaction between JADE1 and 0N terminus tau detected using the corresponding two primary antibodies in the soma (inset). Scale bar, 20 μm

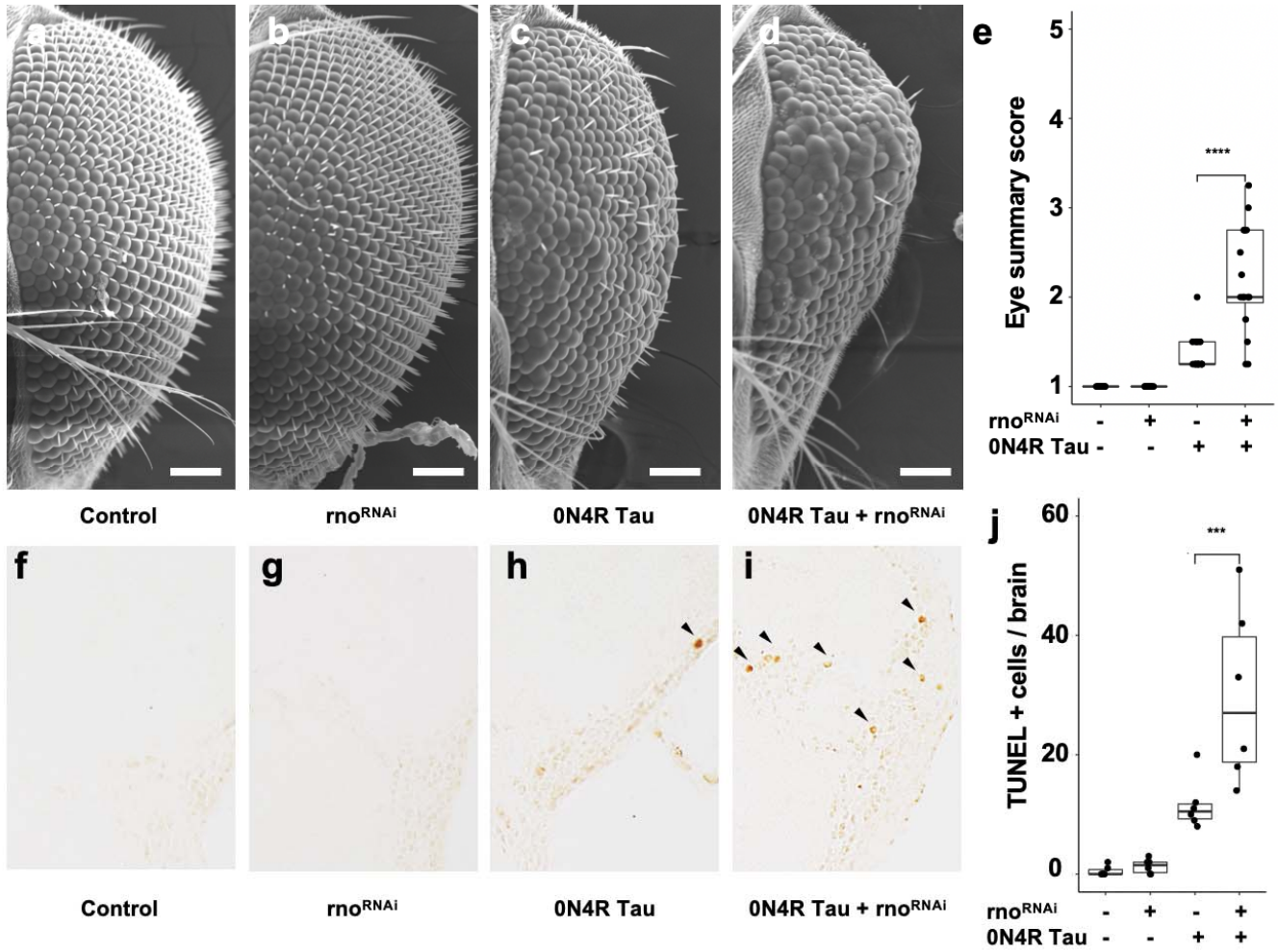

Fig. 5 | RNAi-mediated knockdown of rno enhances tau-induced rough eye and neurotoxicity in the adult *Drosophila* brain. (**a-e**) Rno^{RNAi} significantly enhances the tau-induced rough eye phenotype based on size, roughness, shape, and conical shape (p=8.7 ×10^{-5}). (**f-j**) Rno^{RNAi} significantly enhances levels of terminal deoxynucleotidyl transferase dUTP nick end-labeling (TUNEL) in tau transgenic *Drosophila* compared to tau expressed alone (p=0.008). TUNEL was performed at day 10 of adulthood. An equal number of male and female flies were used for each experiment.

References:

1 Crary, J. F. *et al.* Primary age-related tauopathy (PART): a common pathology associated with human aging. *Acta neuropathologica* **128**, 755-766, doi:10.1007/s00401-014-1349-0 (2014).

2 Ikeda, K. *et al.* Clinical aspects of 'senile dementia of the tangle type' - A subset of dementia in the senium separable from late-onset Alzheimer's disease. *Dement Geriatr Cogn* **10**, 6-11, doi:Doi 10.1159/000017091 (1999).

3 Yamada, M. Senile dementia of the neurofibrillary tangle type (tangle-only dementia): Neuropathological criteria and clinical guidelines for diagnosis. *Neuropathology* **23**, 311-317, doi:DOI 10.1046/j.1440-1789.2003.00522.x (2003).

4 Ikeda, K. *et al.* Clinical aspects of 'senile dementia of the tangle type'-- a subset of dementia in the senium separable from late-onset Alzheimer's disease. *Dement Geriatr Cogn Disord* **10**, 6-11, doi:10.1159/000017091 (1999).

5 Nelson, P. T. *et al.* Brains with medial temporal lobe neurofibrillary tangles but no neuritic amyloid plaques are a diagnostic dilemma but may have pathogenetic aspects distinct from Alzheimer disease. *J Neuropathol Exp Neurol* **68**, 774-784, doi:10.1097/NEN.0b013e3181aacbe9 (2009).

6 Bell, W. R. *et al.* Neuropathologic, genetic, and longitudinal cognitive profiles in primary age-related tauopathy (PART) and Alzheimer's disease. *Alzheimers Dement* **15**, 8-16, doi:10.1016/j.jalz.2018.07.215 (2019).

7 Besser, L. M. *et al.* Differences in Cognitive Impairment in Primary Age-Related Tauopathy Versus Alzheimer Disease. *J Neuropath Exp Neur* **78**, 219-228, doi:10.1093/jnen/nly132 (2019).

8 Janocko, N. J. *et al.* Neuropathologically defined subtypes of Alzheimer's disease differ significantly from neurofibrillary tangle-predominant dementia. *Acta Neuropathol* **124**, 681-692, doi:10.1007/s00401-012-1044-y (2012).

9 Jellinger, K. A. & Attems, J. Prevalence and pathology of vascular dementia in the oldest-old. *J Alzheimers Dis* **21**, 1283-1293 (2010).

10 Nelson, P. T. *et al.* Correlation of Alzheimer disease neuropathologic changes with cognitive status: a review of the literature. *J Neuropathol Exp Neurol* **71**, 362-381, doi:10.1097/NEN.0b013e31825018f7 (2012).

11 Nelson, P. T. *et al.* Clinicopathologic correlations in a large Alzheimer disease center autopsy cohort: neuritic plaques and neurofibrillary tangles "do count" when staging disease severity. *J Neuropathol Exp Neurol* **66**, 1136-1146, doi:10.1097/nen.0b013e31815c5efb (2007).

12 Robinson, J. L. *et al.* Neocortical and hippocampal amyloid-beta and tau measures associate with dementia in the oldest-old. *Brain* **134**, 3708-3715, doi:10.1093/brain/awr308 (2011).

13 Schneider, J. A., Aggarwal, N. T., Barnes, L., Boyle, P. & Bennett, D. A. The Neuropathology of Older Persons with and Without Dementia from Community versus Clinic Cohorts. *Journal of Alzheimers Disease* **18**, 691-701, doi:10.3233/Jad-2009-1227 (2009).

14 Braak, H. & Del Tredici, K. Are cases with tau pathology occurring in the absence of A beta deposits part of the AD-related pathological process? *Acta Neuropathologica* **128**, 767-772, doi:10.1007/s00401-014-1356-1 (2014).

15 Duyckaerts, C. *et al.* PART is part of Alzheimer disease. *Acta Neuropathologica* **129**, 749-756, doi:10.1007/s00401-015-1390-7 (2015).

16 Lafirdeen, A. S. M. *et al.* Biomarker profiles of Alzheimer's disease and dynamic of the association between cerebrospinal fluid levels of beta-amyloid peptide and tau. *PLoS One* **14**, e0217026, doi:10.1371/journal.pone.0217026 (2019).

17 Knopman, D. S. *et al.* Neuropathology of cognitively normal elderly. *J Neuropath Exp Neur* **62**, 1087-1095, doi:DOI 10.1093/jnen/62.11.1087 (2003).

18 Bennett, D. A. *et al.* Neuropathology of older persons without cognitive impairment from two community-based studies. *Neurology* **66**, 1837-1844, doi:DOI 10.1212/01.wnl.0000219668.47116.e6 (2006).

19 Van Cauwenberghe, C., Van Broeckhoven, C. & Sleegers, K. The genetic landscape of Alzheimer disease: clinical implications and perspectives. *Genet Med* **18**, 421-430, doi:10.1038/gim.2015.117 (2016).

20 Hutton, M. *et al.* Association of missense and 5'-splice-site mutations in tau with the inherited dementia FTDP-17. *Nature* **393**, 702-705, doi:10.1038/31508 (1998).

21 Novak, M., Jakes, R., Edwards, P. C., Milstein, C. & Wischik, C. M. Difference between the Tau-Protein of Alzheimer Paired Helical Filament Core and Normal Tau Revealed by Epitope Analysis of

Monoclonal Antibodies-423 and Antibodies-7.51. *P Natl Acad Sci USA* **88**, 5837-5841, doi:DOI 10.1073/pnas.88.13.5837 (1991).

22 Combs, B. & Kanaan, N. M. Exposure of the Amino Terminus of Tau Is a Pathological Event in Multiple Tauopathies. *Am J Pathol* **187**, 1222-1229, doi:10.1016/j.ajpath.2017.01.019 (2017).

23 Jun, G. *et al.* A novel Alzheimer disease locus located near the gene encoding tau protein. *Mol Psychiatry* **21**, 108-117, doi:10.1038/mp.2015.23 (2016).

24 Kouri, N. *et al.* Genome-wide association study of corticobasal degeneration identifies risk variants shared with progressive supranuclear palsy. *Nat Commun* **6**, 7247, doi:10.1038/ncomms8247 (2015).

25 Nalls, M. A. *et al.* Identification of novel risk loci, causal insights, and heritable risk for Parkinson's disease: a meta-analysis of genome-wide association studies. *Lancet Neurol* **18**, 1091-1102, doi:10.1016/S1474-4422(19)30320-5 (2019).

26 Hoglinger, G. U. *et al.* Identification of common variants influencing risk of the tauopathy progressive supranuclear palsy. *Nat Genet* **43**, 699-705, doi:10.1038/ng.859 (2011).

27 Chen, J. A. *et al.* Joint genome-wide association study of progressive supranuclear palsy identifies novel susceptibility loci and genetic correlation to neurodegenerative diseases. *Mol Neurodegener* **13**, 41, doi:10.1186/s13024-018-0270-8 (2018).

28 Santa-Maria, I. *et al.* The MAPT H1 haplotype is associated with tangle-predominant dementia. *Acta neuropathologica* **124**, 693-704, doi:10.1007/s00401-012-1017-1 (2012).

29 Mungas, D., Tractenberg, R., Schneider, J. A., Crane, P. K. & Bennett, D. A. A 2-process model for neuropathology of Alzheimer's disease. *Neurobiol Aging* **35**, 301-308, doi:10.1016/j.neurobiolaging.2013.08.007 (2014).

30 Nelson, P. T. *et al.* Brains With Medial Temporal Lobe Neurofibrillary Tangles But No Neuritic Amyloid Plaques Are a Diagnostic Dilemma But May Have Pathogenetic Aspects Distinct From Alzheimer Disease. *J Neuropath Exp Neur* **68**, 774-784, doi:DOI 10.1097/NEN.0b013e3181aacbe9 (2009).

31 Janocko, N. J. *et al.* Neuropathologically defined subtypes of Alzheimer's disease differ significantly from neurofibrillary tangle-predominant dementia. *Acta Neuropathologica* **124**, 681-692, doi:10.1007/s00401-012-1044-y (2012).

32 Jansen, I. E. *et al.* Genome-wide meta-analysis identifies new loci and functional pathways influencing Alzheimer's disease risk. *Nat Genet* **51**, 404-413, doi:10.1038/s41588-018-0311-9 (2019).

33 McMillan, C. T. *et al.* Alzheimer's genetic risk is reduced in primary age-related tauopathy: a potential model of resistance? *Ann Clin Transl Neur* **5**, 927-934, doi:10.1002/acn3.581 (2018).

34 Montine, T. J. *et al.* Multisite assessment of NIA-AA guidelines for the neuropathologic evaluation of Alzheimer's disease. *Alzheimers Dement* **12**, 164-169, doi:10.1016/j.jalz.2015.07.492 (2016).

35 Besser, L. *et al.* Version 3 of the National Alzheimer's Coordinating Center's Uniform Data Set. *Alzheimer Dis Assoc Disord* **32**, 351-358, doi:10.1097/WAD.0000000000000279 (2018).

36 Folstein, M. F., Robins, L. N. & Helzer, J. E. The Mini-Mental State Examination. *Arch Gen Psychiatry* **40**, 812 (1983).

37 Morris, J. C. The Clinical Dementia Rating (CDR): current version and scoring rules. *Neurology* **43**, 2412-2414 (1993).

38 Mirra, S. S. *et al.* The Consortium to Establish a Registry for Alzheimer's Disease (CERAD). Part II. Standardization of the neuropathologic assessment of Alzheimer's disease. *Neurology* **41**, 479-486 (1991).

39 Braak, H. & Braak, E. Staging of Alzheimer's disease-related neurofibrillary changes. *Neurobiol Aging* **16**, 271-278; discussion 278-284, doi:10.1016/0197-4580(95)00021-6 (1995).

40 Walker, J. M. *et al.* Early Selective Vulnerability of the CA2 Hippocampal Subfield in Primary Age-Related Tauopathy. *J Neuropath Exp Neur* **80**, 102-111, doi:10.1093/jnen/nlaa153 (2021).

41 Kovacs, G. G. *et al.* Aging-related tau astrogliopathy (ARTAG): harmonized evaluation strategy. *Acta Neuropathol* **131**, 87-102, doi:10.1007/s00401-015-1509-x (2016).

42 Purcell, S. *et al.* PLINK: A tool set for whole-genome association and population-based linkage analyses. *Am J Hum Genet* **81**, 559-575, doi:10.1086/519795 (2007).

43 Anderson, C. A. *et al.* Data quality control in genetic case-control association studies. *Nat Protoc* **5**, 1564-1573, doi:10.1038/nprot.2010.116 (2010).

44 Price, A. L. *et al.* Principal components analysis corrects for stratification in genome-wide association studies. *Nat Genet* **38**, 904-909, doi:10.1038/ng1847 (2006).

45 Clarke, L. *et al.* The international Genome sample resource (IGSR): A worldwide collection of genome variation incorporating the 1000 Genomes Project data. *Nucleic Acids Res* **45**, D854-D859, doi:10.1093/nar/gkw829 (2017).

46 Das, S. *et al.* Next-generation genotype imputation service and methods. *Nat Genet* **48**, 1284-1287, doi:10.1038/ng.3656 (2016).

47 McCarthy, S. *et al.* A reference panel of 64,976 haplotypes for genotype imputation. *Nat Genet* **48**, 1279-1283, doi:10.1038/ng.3643 (2016).

48 Willer, C. J., Li, Y. & Abecasis, G. R. METAL: fast and efficient meta-analysis of genomewide association scans. *Bioinformatics* **26**, 2190-2191, doi:10.1093/bioinformatics/btq340 (2010).

49 Pruim, R. J. *et al.* LocusZoom: regional visualization of genome-wide association scan results. *Bioinformatics* **26**, 2336-2337, doi:10.1093/bioinformatics/btq419 (2010).

50 Otero-Garcia, M. *et al.* Single-soma transcriptomics of tangle-bearing neurons in Alzheimer's disease reveals the signatures of tau-associated synaptic dysfunction. *bioRxiv*, 2020.2005.2011.088591, doi:10.1101/2020.05.11.088591 (2020).

51 Aldridge, G. M., Podrebarac, D. M., Greenough, W. T. & Weiler, I. J. The use of total protein stains as loading controls: an alternative to high-abundance single-protein controls in semi-quantitative immunoblotting. *J Neurosci Methods* **172**, 250-254, doi:10.1016/j.jneumeth.2008.05.003 (2008).

52 Beecham, G. W. *et al.* Genome-Wide Association Meta-analysis of Neuropathologic Features of Alzheimer's Disease and Related Dementias. *Plos Genet* **10**, doi:ARTN e1004606
10.1371/journal.pgen.1004606 (2014).

53 Hong, S. *et al.* Genome-wide association study of Alzheimer's disease CSF biomarkers in the EMIF-AD Multimodal Biomarker Discovery dataset. *Transl Psychiatry* **10**, 403, doi:10.1038/s41398-020-01074-z (2020).

54 Qi, T. *et al.* Identifying gene targets for brain-related traits using transcriptomic and methylomic data from blood. *Nat Commun* **9**, 2282, doi:10.1038/s41467-018-04558-1 (2018).

55 Wittmann, C. W. *et al.* Tauopathy in Drosophila: Neurodegeneration without neurofibrillary tangles. *Science* **293**, 711-714, doi:DOI 10.1126/science.1062382 (2001).

56 Yokoyama, J. S. *et al.* Shared genetic risk between corticobasal degeneration, progressive supranuclear palsy, and frontotemporal dementia. *Acta Neuropathol* **133**, 825-837, doi:10.1007/s00401-017-1693-y (2017).

57 Jabbari, E. *et al.* Genetic determinants of survival in progressive supranuclear palsy: a genome-wide association study. *Lancet Neurol* **20**, 107-116, doi:10.1016/S1474-4422(20)30394-X (2021).

58 Sanchez-Contreras, M. Y. *et al.* Replication of progressive supranuclear palsy genome-wide association study identifies SLCO1A2 and DUSP10 as new susceptibility loci. *Molecular Neurodegeneration* **13**, doi:ARTN 37
10.1186/s13024-018-0267-3 (2018).

59 Broce, I. *et al.* Immune-related genetic enrichment in frontotemporal dementia: An analysis of genome-wide association studies. *Plos Medicine* **15**, doi:ARTN e1002487
10.1371/journal.pmed.1002487 (2018).

60 Kouri, N. *et al.* Genome-wide association study of corticobasal degeneration identifies risk variants shared with progressive supranuclear palsy. *Nat Commun* **6**, doi:ARTN 7247
10.1038/ncomms8247 (2015).

61 Hoglinger, G. U. *et al.* Identification of common variants influencing risk of the tauopathy progressive supranuclear palsy. *Nat Genet* **43**, 699-U125, doi:10.1038/ng.859 (2011).

62 Zhou, M. I. *et al.* Jade-1, a candidate renal tumor suppressor that promotes apoptosis. *P Natl Acad Sci USA* **102**, 11035-11040, doi:10.1073/pnas.0500757102 (2005).

63 Chitalia, V. C. *et al.* Jade-1 inhibits Wnt signalling by ubiquitylating beta-catenin and mediates Wnt pathway inhibition by pVHL. *Nature Cell Biology* **10**, 1208-1216, doi:10.1038/ncb1781 (2008).

64 Zeng, L. L. *et al.* Candidate Tumor Suppressor and pVHL Partner Jade-1 Binds and Inhibits AKT in Renal Cell Carcinoma. *Cancer Res* **73**, 5371-5380, doi:10.1158/0008-5472.Can-12-4707 (2013).

65 Wesseling, H. *et al.* Tau PTM Profiles Identify Patient Heterogeneity and Stages of Alzheimer's Disease. *Cell* **183**, 1699-+, doi:10.1016/j.cell.2020.10.029 (2020).

66 Sealey, M. A. *et al.* Distinct phenotypes of three-repeat and four-repeat human tau in a transgenic model of tauopathy. *Neurobiol Dis* **105**, 74-83, doi:10.1016/j.nbd.2017.05.003 (2017).

67 Lambert, J. C. *et al.* Meta-analysis of 74,046 individuals identifies 11 new susceptibility loci for Alzheimer's disease. *Nat Genet* **45**, 1452-1458, doi:10.1038/ng.2802 (2013).

68 Marioni, R. E. *et al.* GWAS on family history of Alzheimer's disease. *Transl Psychiatry* **8**, 99, doi:10.1038/s41398-018-0150-6 (2018).

69 Kunkle, B. W. *et al.* Genetic meta-analysis of diagnosed Alzheimer's disease identifies new risk loci and implicates Abeta, tau, immunity and lipid processing. *Nat Genet* **51**, 414-430, doi:10.1038/s41588-019-0358-2 (2019).

70 Andrews, S. J., Fulton-Howard, B. & Goate, A. Interpretation of risk loci from genome-wide association studies of Alzheimer's disease. *Lancet Neurol* **19**, 326-335, doi:10.1016/S1474-4422(19)30435-1 (2020).

71 Ikeda, K. *et al.* A subset of senile dementia with high incidence of the apolipoprotein E epsilon2 allele. *Ann Neurol* **41**, 693-695, doi:10.1002/ana.410410522 (1997).

72 Jellinger, K. A. & Attems, J. Neurofibrillary tangle-predominant dementia: Comparison with classical Alzheimer disease. *Acta Neuropathologica* **113**, 107-117, doi:10.1007/s00401-006-0156-7 (2007).

73 Reiman, E. M. *et al.* Exceptionally low likelihood of Alzheimer's dementia in APOE2 homozygotes from a 5,000-person neuropathological study. *Nat Commun* **11**, doi:ARTN 667 10.1038/s41467-019-14279-8 (2020).

74 Besser, L. M., Crary, J. F., Mock, C. & Kukull, W. A. Comparison of symptomatic and asymptomatic persons with primary age-related tauopathy. *Neurology* **89**, 1707-1715, doi:10.1212/WNL.0000000000004521 (2017).

75 Shi, Y. *et al.* ApoE4 markedly exacerbates tau-mediated neurodegeneration in a mouse model of tauopathy. *Nature* **549**, 523-+, doi:10.1038/nature24016 (2017).

76 Abner, E. L. *et al.* Diffuse Amyloid-beta Plaques, Neurofibrillary Tangles, and the Impact of APOE in Elderly Persons' Brains Lacking Neuritic Amyloid Plaques. *Journal of Alzheimers Disease* **64**, 1307-1324, doi:10.3233/Jad-180514 (2018).

77 Farfel, J. M., Yu, L., De Jager, P. L., Schneider, J. A. & Bennett, D. A. Association of APOE with tau-tangle pathology with and without beta-amyloid. *Neurobiol Aging* **37**, 19-25, doi:10.1016/j.neurobiolaging.2015.09.011 (2016).

78 Strickland, S. L. *et al.* MAPT haplotype-stratified GWAS reveals differential association for AD risk variants. *Alzheimers Dement* **16**, 983-1002, doi:10.1002/alz.12099 (2020).

79 Sanchez-Juan, P. *et al.* The MAPT H1 Haplotype Is a Risk Factor for Alzheimer's Disease in APOE epsilon 4 Non-carriers. *Front Aging Neurosci* **11**, doi:ARTN 327 10.3389/fnagi.2019.00327 (2019).

80 Myers, A. J. *et al.* The H1c haplotype at the MAPT locus is associated with Alzheimer's disease. *Human Molecular Genetics* **14**, 2399-2404, doi:10.1093/hmg/ddi241 (2005).

81 Boettger, L. M., Handsaker, R. E., Zody, M. C. & McCarroll, S. A. Structural haplotypes and recent evolution of the human 17q21.31 region. *Nat Genet* **44**, 881-+, doi:10.1038/ng.2334 (2012).

82 Steinberg, K. M. *et al.* Structural diversity and African origin of the 17q21.31 inversion polymorphism. *Nat Genet* **44**, 872-+, doi:10.1038/ng.2335 (2012).

83 Stutzbach, L. D. *et al.* The unfolded protein response is activated in disease-affected brain regions in progressive supranuclear palsy and Alzheimer's disease. *Acta Neuropathol Com* **1**, doi:Artn 31 10.1186/2051-5960-1-31 (2013).

84 Smith, H. L. & Mallucci, G. R. The unfolded protein response: mechanisms and therapy of neurodegeneration. *Brain* **139**, 2113-2121, doi:10.1093/brain/aww101 (2016).

85 Larsson, M. *et al.* GWAS findings for human iris patterns: associations with variants in genes that influence normal neuronal pattern development. *Am J Hum Genet* **89**, 334-343, doi:10.1016/j.ajhg.2011.07.011 (2011).

86 Yu, L. *et al.* Association of Brain DNA methylation in SORL1, ABCA7, HLA-DRB5, SLC24A4, and BIN1 with pathological diagnosis of Alzheimer disease. *JAMA Neurol* **72**, 15-24, doi:10.1001/jamaneurol.2014.3049 (2015).

87 Efthymiou, A. G. & Goate, A. M. Late onset Alzheimer's disease genetics implicates microglial pathways in disease risk. *Mol Neurodegener* **12**, 43, doi:10.1186/s13024-017-0184-x (2017).

88 Holmes, B. B. *et al.* Heparan sulfate proteoglycans mediate internalization and propagation of specific proteopathic seeds. *P Natl Acad Sci USA* **110**, E3138-E3147, doi:10.1073/pnas.1301440110 (2013).

89 Lambert, J. C. *et al.* Meta-analysis of 74,046 individuals identifies 11 new susceptibility loci for Alzheimer's disease. *Nat Genet* **45**, 1452-U1206, doi:10.1038/ng.2802 (2013).
90 Beecham, G. W. Genome-Wide Association Meta-analysis of Neuropathologic Features of Alzheimer's Disease and Related Dementias (vol 10, e1004606, 2014). *Plos Genet* **10**, doi:ARTN e1004867
10.1371/journal.pgen.1004867 (2014).
91 Zhou, Y. *et al.* Human and mouse single-nucleus transcriptomics reveal TREM2-dependent and TREM2-independent cellular responses in Alzheimer's disease. *Nat Med* **26**, 131-142, doi:10.1038/s41591-019-0695-9 (2020).
92 Lee, S. H. *et al.* Trem2 restrains the enhancement of tau accumulation and neurodegeneration by beta-amyloid pathology. *Neuron* **109**, 1283-1301 e1286, doi:10.1016/j.neuron.2021.02.010 (2021).
93 Keren-Shaul, H. *et al.* A Unique Microglia Type Associated with Restricting Development of Alzheimer's Disease. *Cell* **169**, 1276-1290 e1217, doi:10.1016/j.cell.2017.05.018 (2017).
94 Dregni, A. J. *et al.* In vitro 0N4R tau fibrils contain a monomorphic beta-sheet core enclosed by dynamically heterogeneous fuzzy coat segments. *Proc Natl Acad Sci U S A* **116**, 16357-16366, doi:10.1073/pnas.1906839116 (2019).
95 Fitzpatrick, A. W. P. *et al.* Cryo-EM structures of tau filaments from Alzheimer's disease. *Nature* **547**, 185-190, doi:10.1038/nature23002 (2017).
96 Scheres, S. H., Zhang, W., Falcon, B. & Goedert, M. Cryo-EM structures of tau filaments. *Curr Opin Struct Biol* **64**, 17-25, doi:10.1016/j.sbi.2020.05.011 (2020).
97 Wesseling, H. *et al.* Tau PTM Profiles Identify Patient Heterogeneity and Stages of Alzheimer's Disease. *Cell* **183**, 1699-1713 e1613, doi:10.1016/j.cell.2020.10.029 (2020).
98 Braak, E., Braak, H. & Mandelkow, E. M. A sequence of cytoskeleton changes related to the formation of neurofibrillary tangles and neuropil threads. *Acta neuropathologica* **87**, 554-567, doi:10.1007/BF00293315 (1994).
99 Boone, D. K. *et al.* Evidence linking microRNA suppression of essential prosurvival genes with hippocampal cell death after traumatic brain injury. *Sci Rep* **7**, 6645, doi:10.1038/s41598-017-06341-6 (2017).
100 Chitalia, V. C. *et al.* Jade-1 inhibits Wnt signalling by ubiquitylating beta-catenin and mediates Wnt pathway inhibition by pVHL. *Nat Cell Biol* **10**, 1208-1216, doi:10.1038/ncb1781 (2008).
101 Siriwardana, N. S., Meyer, R., Havasi, A., Dominguez, I. & Panchenko, M. V. Cell cycle-dependent chromatin shuttling of HBO1-JADE1 histone acetyl transferase (HAT) complex. *Cell Cycle* **13**, 1885-1901, doi:10.4161/cc.28759 (2014).
102 Panchenko, M. V. Structure, function and regulation of jade family PHD finger 1 (JADE1). *Gene* **589**, 1-11, doi:10.1016/j.gene.2016.05.002 (2016).
103 Borgal, L. *et al.* The ciliary protein nephrocystin-4 translocates the canonical Wnt regulator Jade-1 to the nucleus to negatively regulate beta-catenin signaling. *J Biol Chem* **287**, 25370-25380, doi:10.1074/jbc.M112.385658 (2012).
104 Voas, M. G. & Rebay, I. The novel plant homeodomain protein rhinoceros antagonizes Ras signaling in the Drosophila eye. *Genetics* **165**, 1993-2006 (2003).
105 Zhou, M. I. *et al.* The von Hippel-Lindau tumor suppressor stabilizes novel plant homeodomain protein Jade-1. *J Biol Chem* **277**, 39887-39898, doi:10.1074/jbc.M205040200 (2002).
106 Lisztwan, J., Imbert, G., Wirbelauer, C., Gstaiger, M. & Krek, W. The von Hippel-Lindau tumor suppressor protein is a component of an E3 ubiquitin-protein ligase activity. *Gene Dev* **13**, 1822-1833, doi:DOI 10.1101/gad.13.14.1822 (1999).
107 Silva, M. C. *et al.* Targeted degradation of aberrant tau in frontotemporal dementia patient-derived neuronal cell models. *Elife* **8**, doi:ARTN e45457
10.7554/eLife.45457 (2019).
108 Nagy, Z. *et al.* Staging of Alzheimer-type pathology: An interrater-intrarater study. *Dement Geriatr Cogn* **8**, 248-251, doi:Doi 10.1159/000106639 (1997).
109 Iida, M. A. *et al.* Predictors of cognitive impairment in primary age-related tauopathy: an autopsy study. *bioRxiv*, 2021.2006.2008.447553, doi:10.1101/2021.06.08.447553 (2021).
110 Congdon, E. E. & Sigurdsson, E. M. Tau-targeting therapies for Alzheimer disease. *Nat Rev Neurol* **14**, 399-415, doi:10.1038/s41582-018-0013-z (2018).